ARL

US Army Research Laboratory

2nd Annual Postdoc Research Day: US Army Research Laboratory Poster Symposia and Activities

by Efraín Hernández–Rivera, Julia Cline, and Milena B Graziano

NOTICES

Disclaimers

The findings in this report are not to be construed as an official Department of the Army position unless so designated by other authorized documents.

Citation of manufacturer's or trade names does not constitute an official endorsement or approval of the use thereof.

Destroy this report when it is no longer needed. Do not return it to the originator.

ARL

US Army Research Laboratory

2nd Annual Postdoc Research Day: US Army Research Laboratory Poster Symposia and Activities

by Efraín Hernández–Rivera
Weapons and Materials Research Directorate, ARL

Julia Cline
Oak Ridge Institute for Science and Education, Oak Ridge, TN

Milena B Graziano
Oak Ridge Associated Universities, Oak Ridge, TN

REPORT DOCUMENTATION PAGE

Public reporting burden for this collection of information is estimated to average 1 hour per response, including the time for reviewing instructions, searching existing data sources, gathering and maintaining the data needed, and completing and reviewing the collection information. Send comments regarding this burden estimate or any other aspect of this collection of information, including suggestions for reducing the burden, to Department of Defense, Washington Headquarters Services, Directorate for Information Operations and Reports (0704-0188), 1215 Jefferson Davis Highway, Suite 1204, Arlington, VA 22202-4302. Respondents should be aware that notwithstanding any other provision of law, no person shall be subject to any penalty for failing to comply with a collection of information if it does not display a currently valid OMB control number.
PLEASE DO NOT RETURN YOUR FORM TO THE ABOVE ADDRESS.

1. REPORT DATE *(DD-MM-YYYY)*	2. REPORT TYPE	3. DATES COVERED *(From - To)*
April 2018	Special Report	September 2017

4. TITLE AND SUBTITLE
2nd Annual Postdoc Research Day: US Army Research Laboratory Poster Symposia and Activities

5a. CONTRACT NUMBER

5b. GRANT NUMBER

5c. PROGRAM ELEMENT NUMBER

6. AUTHOR(S)
Efraín Hernández–Rivera, Julia Cline, and Milena B Graziano

5d. PROJECT NUMBER

5e. TASK NUMBER

5f. WORK UNIT NUMBER

7. PERFORMING ORGANIZATION NAME(S) AND ADDRESS(ES)
US Army Research Laboratory
ATTN: RDRL-WMM-B
Aberdeen Proving Ground, MD 21005-5066

8. PERFORMING ORGANIZATION REPORT NUMBER
ARL-SR-0394

9. SPONSORING/MONITORING AGENCY NAME(S) AND ADDRESS(ES)

10. SPONSOR/MONITOR'S ACRONYM(S)

11. SPONSOR/MONITOR'S REPORT NUMBER(S)

12. DISTRIBUTION/AVAILABILITY STATEMENT
Approved for public release; distribution is unlimited.

13. SUPPLEMENTARY NOTES
primary author's email: <efrain.hernandez18.civ@mail.mil>.

14. ABSTRACT
The US Army Research Laboratory (ARL) Postdoc Association (PDA) organized its 2nd Annual Postdoc Research Day to showcase postdoctoral achievements and contributions across the enterprise. The event included an invited speaker (in a joint session with ARL's 25th Anniversary keynote series), a Q&A panel, and a poster session.

This special report contains a brief summary outlining the event and the current status of ARL's postdoctoral research community. The contributed abstracts presented at the event and a limited number of contributed posters are appended.

15. SUBJECT TERMS
ARL Postdoc Research Day, Postdoc Association, 2017 National Postdoc Week, ARL 25th Anniversary, Poster Symposia

16. SECURITY CLASSIFICATION OF:			17. LIMITATION OF ABSTRACT	18. NUMBER OF PAGES	19a. NAME OF RESPONSIBLE PERSON
a. REPORT Unclassified	**b. ABSTRACT** Unclassified	**c. THIS PAGE** Unclassified	UU	48	Efraín Hernández–Rivera
					19b. TELEPHONE NUMBER (Include area code) 410-306-4961

Contents

List of Figures

List of Tables

Acknowledgments

The 2nd Annual Postdoc Research Organizing Committee would like to thank the dedicated work and support of US Army Research Laboratory's (ARL's) administrative staff. These include, but are not limited to, Ms Jenna C Brady, Mr Micah J Smith, and countless others. The committee would also like to thank the ARL Fellows and S&T leaders (Dr Richard C Becker, Dr John D Clayton, Dr Brad E Forch, Dr Piotr J Franaszczuk, Dr Mary P Harper, Dr Rose A Pesce–Rodriguez, Dr Shashi P Karna, and Dr Ananthram Swami) who volunteered their time to judge the poster session. Lastly, we want to thank the panelists (Dr Troy A Alexander, Dr Brendan Hanrahan, and Dr Rose A Pesce–Rodriguez) for a great Q&A session.

Lastly, we must recognize the 2nd Annual Postdoc Research Day (2PRD) Organizing Committee, which was formed by a group of dedicated volunteer postdocs. Their hard work enabled the success of the 2PRD.

- Milena B Graziano[1] (SEDD)

- Efraín Hernández–Rivera[1] (WMRD)

- Aimable Kalume (CISD)

- Dominika N Lastovickova (WMRD)

- Meagan C Small (SEDD)

- Gosia Turalska (OC/SEDD)

- Theresah Zu (SEDD)

---

[1]Event co-chair

1. Introduction

The 2nd Annual Postdoc Research Day (2PRD) is a US Army Research Laboratory (ARL) Postdoc Association (PDA) initiative to commemorate postdoctoral executed and lead research across ARL. It was planned to coincide with the 2017 National Postdoc Week in celebration of ARL's postdoctoral cohort. The goal is to bring awareness to the important research being performed by postdocs and further promote collaboration where suited. Mainly, the 2PRD is a venue to celebrate and promote the postdoctoral experience at ARL.

This was the second iteration of this event and was held on 19 September 2017 at ARL's Laboratory Center in Adelphi, Maryland. The 2PRD included a panel session where postdoctoral fellows were able to interact with current ARL civilians with a diverse perspective of what enables success at ARL. The panelists started their careers as ARL postdocs themselves and brought a unique and rich perspective to the topic. A total of 26 postdocs presented posters, and many others attended other activities like the Q&A panel with current ARL civilians.

The 2PRD objectives were as follows:

- Recognize postdocs' contributions to current state-of-the-art research and discovery at ARL.

- Foster collaborative research amongst postdocs with common research interests.

- Serve as an interactive platform for postdocs and upper management.

This Special Report provides a snapshot of the 2PRD. An abstract book and limited number of contributed posters are published as Appendixes.

2. Engagement Across the Laboratory

A total of 26 postdocs presented posters, and these are listed in Table 1 with their location and directorate affiliation. Directorate-specific participation is graphically shown in Fig. 1. It is encouraging to see that participation from the Aberdeen Proving Ground (APG) postdoctoral staff was not affected by the event taking place at Adelphi Laboratory Center (ALC). This speaks to both postdoctoral interest, and

mentor and management support of the postdoctoral cohorts. The abstract book created to advertise the event has been appended at the end of the report, Appendix A. A limited number of contributed posters can be found in Appendix B.

Table 1 List of postdoctoral fellows who presented at the symposia

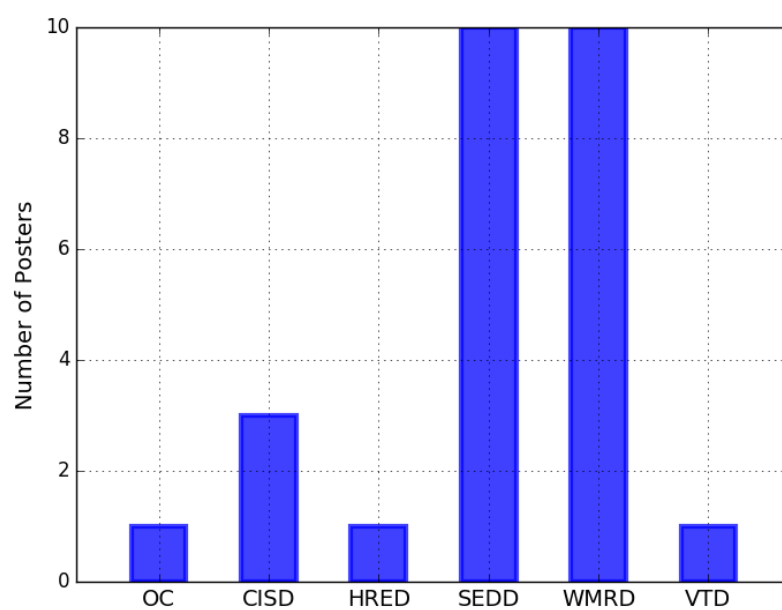| Presenter	Directorate	Location
Boltersdorf, Jonathan	SEDD	ALC
Cline, Julia	WMRD	APG
Cox, Kevin	SEDD	ALC
Drnec, Kim	HRED	APG
Golter, David	SEDD	ALC
Graziano, Milena	SEDD	ALC
Gutstein, Steven	CISD	ALC
Hampton, Carolyn	WMRD	APG
Hernandez, Efrain	WMRD	APG
Hofmeister, Clara	WMRD	APG
Jackson, Marc	CISD	APG
Kalume, Aimable	CISD	ALC
Ku, Nicholas	WMRD	APG
Lafond, Patrick	WMRD	APG
Llopis-Jepsen, Antonio	SEDD	ALC
Magagnosc, Daniel	WMRD	APG
Mahoney, Luther	SEDD	ALC
Nguyen, Quang	OC	ALC
Nogar, Stephen	VTD	APG
Roenbeck, Michael	WMRD	APG
Schroeder, Marshall	SEDD	ALC
Shoulders, William	WMRD	APG
Small, Meagan	SEDD	APG
Tseng, Victor	SEDD	ALC
Wilson, Adam	SEDD	ALC
Yeager, Michael	WMRD	APG

Fig. 1 Directorate-level participation of postdoctoral poster presenters

INTENTIONALLY LEFT BLANK.

Appendix A. Contributed Abstracts Presented at the 2nd Postdoc Research Day

The PostDoctoral Association's
2nd Annual ARL Postdoc Research Day

ABSTRACT BOOK

19 Sep 2017
Adelphi, MD

This page is intentionally left blank
Document typeset with LaTeX

Electrochemical Performance of Lithium-ion Capacitors Evaluated under High Temperature and High Voltage Stress using Redox Stable Electrolytes and Additives

Boltersdorf, J.[1], Delp, S.A.[1,2], Yan, J.[3,4], Cao, B.[3], Zheng, J.P.[4] and Jow, T.R.[1]

[1]United States Army Research Laboratory, **RDRL-SED-C**, Adelphi, MD, [2]General Technical Services, Adelphi, MD, [3]General Capacitor LLC & INTL, INC. Tallahassee, FL, [4]Department of Electrical and Computer Engineering, Florida A&M University-Florida State University, Tallahassee, FL

*corresp. author: jonathan.a.boltersdorf.ctr@mail.mil

Lithium-ion capacitors (LICs) were investigated for high power, moderate energy density applications for operation in extreme environments with prolonged cycle-life performance. The LICs were assembled as three-layered pouch cells in an asymmetric configuration employing Faradaic pre-lithiated hard carbon anodes and non-Faradaic ion adsorption-desorption activated carbon (AC) cathodes. The capacity retention was measured under high stress conditions, while the design factor explored was electrolyte formulation using a set of carbonates and electrolyte additives, with a focus on their stability. The LIC cells were evaluated using critical performance tests under the following high stress conditions: long-term voltage floating-cycling stability at room temperature (2.2-3.8 V), high temperature storage at 3.8 V, and charge voltages up to 4.4 V. The rate performance of different electrolytes and additives was measured after the initial LIC cell formation for a 1C to 10C rate. The presence of vinylene carbonate (VC) and tris (trimethylsilyl) phosphate (TMSP) were found to be essential to the improved electrochemical performance of the LIC cells under all testing conditions.

Comparison of the in-plane shear behavior of UHMWPE fiber and highly oriented tape composites

Cline, J.[1], Bogetti, T.[1] and Love, B.[1]

[1]United States Army Research Laboratory, **RDRL-WMM-B**, APG, MD

*corresp. author: julia.cline.ctr@mail.mil

Highly oriented solid state extruded polyethylene (PE) tape composites, an emerging form of ultra-high molecular weight polyethylene (UHMWPE), are a promising candidate to enhance the ballistic performance of lightweight protective systems. It is hypothesized that the in-plane shear modulus, G12, is an order of magnitude larger for solid state extruded polyethylene films than gel-spun polyethylene fibers. In-plane behavior is widely known to affect ballistic performance. The focus of this work is to experimentally measure the in-plane shear behavior for an UHMWPE fiber material system (SR3136) and a tape system (Tensylon 30A) using tensile tests of specimens with a [45] layup. The results will be used to draw conclusions of the difference of in-plane response between fiber and tape PE material systems. As PE composite materials are highly sensitive to processing conditions, the effect of applied temperature and pressure during consolidation on the in-plane response will be investigated.

Quantum Measurement and Networking with Rubidium Atoms

Cox, K.[1]

[1]United States Army Research Laboratory, **RDRL-SEE-E**, Adelphi, MD

*corresp. author: kevin.c.cox29.ctr@mail.mil

In the Neutral Atom Quantum Science Lab, we develop prototype systems that harness the unique features of quantum mechanics for next-generation Army capabilities in precision measurement and networking. In this poster, I will present how we are using an ensemble of 1 million rubidium atoms, cooled to temperatures near absolute zero and trapped within laser beams, to store and read out quantum bits of information in new ways. I will also give context for how our research may lead to detection of fields with extreme sensitivity and a "quantum internet".

Predicting human automation interaction in the context of human agent teaming

Drnec, K.[1], Carter, E.[1], Gremillion, G.[1], Estepp, J.[1], Metcalfe, J.S.[1], Nothwang, W.[1] and Marathe, A.[1]

[1]United States Army Research Laboratory, **RDRL-HRF-B**, APG, MD

*corresp. author: kim.a.drnec2.ctr@mail.mil

Human agent teams have yet to reach anticipated levels of performance. A key reason is that the human operator makes poor decisions about how and when to interact with a given automation resulting in misuse. Although trust in automation has long been considered to underlie appropriate use of an automation, recent research has questioned this premise and has focused on defining and predicting human interaction behavior. If an interaction can be predicted and considered inappropriate given the context, mitigation might be possible and human agent team performance can be improved. We set out to determine if a set of environmental, task-based, and psychophysiological features can be used to predict interaction up to three seconds before it occurs. We were able to predict when the subject was about to take over control or hand control back to the automation above chance on average. Future work is planned in which the classifiers are used in real time and to actuate cues that could mitigate inappropriate interaction behavior.

Optically Induced Switching of Charged States of Defects in 4H-SiC

Golter, D.A.[1] and Lai, W.[1]

[1]United States Army Research Laboratory, **RDRL-SEE-E**, Adelphi, MD

*corresp. author: david.a.golter.ctr@mail.mil

In the Solid State Quantum Lab we study solid-state defect qubits for quantum information and sensing applications. Optical and microwave excitation allow us to probe and control electron and nuclear spins, measuring coherence times and mapping energy level structures for these "artificial atoms". We evaluate different host materials and defect types for their potential use in quantum networking entanglement schemes as well as for building high precision nano-sensors.

In this poster we present our work studying divacancy defects in silicon carbide. Photoluminescence excitation mea-

surements identify optimal excitation energies. For an energy below 1.3 eV the photoluminescence is suppressed by more than two orders of magnitude and is recovered in the presence of a higher energy repumping laser. We interpret this as optically driven switching between bright and dark charged states. This process can lead to spectral diffusion but can also be exploited for long-term data storage or nuclear-spin based quantum memory.

Determination of Partial Ordering in Pseudomorphic AlGaN Films Grown on AlN Single Crystals

Graziano, M.B.[1]*,Tompkins, R.P.*[1] *and Jones, K.A.*[1]

[1]United States Army Research Laboratory, **RDRL-SED-E**, Adelphi, MD

*corresp. author: milena.b.graziano.ctr@mail.mil

Three-wave X-ray multiple diffraction was used to investigate the structural properties of AlGaN films grown on low defect density AlN substrates using metallorganic chemical vapor deposition. The scans were recorded using the Renninger scheme set to the primary (0001) forbidden reflection. As the samples were rotated about the surface normal, the visibility of several three-wave X-ray combination peaks was achieved, attributed to the high crystallinity of the films. The position, shape and relative intensities of the resolved multiple diffraction peaks (MPs) were analyzed for differently aligned Renninger curves in order to distinguish normal and hybrid XRMD paths. The effects of AlN wafer curvature and AlGaN crystallographic tilt on Renninger diagrams are presented and discussed. For pseudomorphic alloys, the appearance of the AlGaN (0001) Bragg reflection was identified at sample azimuth positions away from those corresponding to MPs. The existence of this reflection is attributed to partial ordering of the solid solution, which has not been explored as a strain-induced effect in AlGaN materials. This phenomenon is unrelated to commonly reported alloy film compositional inhomogeneity, as the surface morphology was atomically smooth, free of macrostepped features. As such, the occurrence of atomic ordering is potentially a response to the residual built-in film strain, which can have significant impact on the electronic structure and optical properties of the alloys.

Optimal Output Codes For Deep Convolutional Neural Nets

Gutstein, S.[1] *and Stump, E.*[1]

[1]United States Army Research Laboratory, **RDRL-CII-A**, Adelphi, MD

*corresp. author: steven.m.gutstein.ctr@mail.mil

The choice of output encoding influences a neural net's ability to learn source tasks, engage in transfer learning and to avoid catastrophic forgetting. All of these metrics are relevant to a neural net's ability to engage in lifelong learning and can be used to evaluate an encoding's effectiveness. Although 1-Hot encoding is used by the vast majority of practitioners for training neural nets, it is not an optimal technique.

This work examines encodings that are superior to 1-Hot encodings with respect to all 3 of the above metrics. One such encoding is the random error correcting output code, which has been known in machine learning since its introduction by Bakiri & Dieterrich about 25 years ago. Other codes examined in this talk are based upon siamese similarity encodings (SSE), which were developed for this work. SSEs were par-

tially inspired by the success of semantic codes for zero-shot learning.

Unlike semantic codes, SSEs are not hand-crafted and do not depend upon the expressiveness of natural languages or the linguistic skill of the trainer of a net. This should make them applicable to a broader range of problems than semantic encodings. Finally, we also explored the use of latent codes for transfer learning. Because these codes are passively acquired while learning source tasks, they have a 'zero - shot' quality to them, and if specifically trained are extremely resistant to catastrophic forgetting. Experiments comparing the efficacy of 1-Hot, random error correcting output, siamese similarity and latent encoding techniques were carried out using the CIFAR-100 dataset and NIST Special Dataset 19.

Finite Element Analysis of Protective Footwear

Hampton, C.[1] *and Kleinberger, M.*[1]

[1]United States Army Research Laboratory, **RDRL-WMP-B**, APG, MD

*corresp. author: carolyn.e.hampton.ctr@mail.mil

82% of active combat musculoskeletal injuries in the Army were attributed to underbody blast exposure. 18.5% of these injuries are lower extremity fractures which hinder Army readiness and can incur long-term disability. This study improves upon prior research investigating the injury mechanisms and the effectiveness of protective footwear. In brief, an improved finite element human leg model created from CT geometry data from an average sized male volunteer was combined with a combat boot finite element model. Paired booted and unbooted axial pendulum impacts at 5, 7, and 10 m/s, representing mounted underbody blast scenarios, were simulated to collect tibial force data and stress concentrations and compared against experimental data. Peak forces were 6% higher than the experimental data on average, and CORA curve correlation scores were 0.86 on a scale of 0 to 1. Boot usage offered roughly 1/3 mitigation of peak force. Variations in the foot arch structure and material properties of the soft tissue were found to influence the results. These findings highlight the ability of the finite element method to quickly develop and assess personalized protective equipment but care must be taken when interpreting the results in the context of the broader Army population.

Design of Experiments Approach to Optimizing Complex Bond Order and Reactive Potentials

Hernández–Rivera, E.[1]*, Chowdhury, S.*[2]*, Tschopp, M.A.*[1] *and Coleman, S.P.*[1]

[1]United States Army Research Laboratory, **RDRL-WMM-F**, APG, MD, [2]Department of Mechanical and Aerospace Engineering, University at Buffalo, Buffalo, NY

*corresp. author: efrain.hernandez18.ctr@mail.mil

In order to understand fundamental materials behavior, we often rely on atomistic calculations. A popular approach is to use molecular dynamics (MD), which can be extended into much larger length and time scales than first principles methods. However, any MD simulation and knowledge gained from it is detrimentally limited by the accuracy of the interatomic potential used. Parameterization and optimization of complex interatomic potentials can become a main challenge and bottleneck for computational materials scientist. Furthermore,

optimization can become a prohibitively expensive procedure for some of the more complex potentials that contain hundreds of fitting parameters, e.g. ReaxFF.

We have developed a systematic approach that relies on statistical knowledge obtained from designs of experiments to overcome this optimization barriers. The approach consists of a pre-optimization sensitivity analysis which enables us to efficiently identify essential parameters and analytically reduce our computational domain. With this reduced domain, we apply Latin Hypercube Sampling in designing our computational experiments to develop surrogate models. These metamodels are then employed in the multi-objective optimization schemes, which yield an optimized set of parameters. Validating these optimized parameterizations shows that this approach can efficiently be used to optimize complex interatomic potentials.

Effect of a mid-build halt on the microstructure and porosity in powder bed fusion stainless steel parts

Hofmeister, C.[1], Kudzal, A.[1,2], Taggart-Scarff, J.[1], Rogers, R.[3], Sietins, J.[1] and McWilliams, B.[1]

[1]United States Army Research Laboratory, **RDRL-WMM-D**, APG, MD, [2]Worcester Polytechnic Institute, Worcester, MA, [3]Dynamic Science Inc, Phoenix, AZ

*corresp. author: clara.m.hofmeister.ctr@mail.mil

Interruption of builds during powder bed fusion (PBF) can occur if part or power failure occurs. An interruption of the build cycle may create a highly porous plane visible from the outside surface of the part known as a witness line. The effect of witness lines on the microstructure of the part is unknown. In this study, the PBF of 17-4 stainless steel powder was intentionally halted mid-build for hold times ranging from 5 min to 12 hours and then allowed to continue. Microscopy and x-ray microcomputed tomography were conducted to determine the effect of hold time on the microstructure of the newly created heat affected zone as well as the size and morphology of the porosity in each witness line. The formation of witness lines and its effect on the quality of manufactured parts will be discussed.

Detection of Enemy Threats and the Impact of Asset Information on Decision Making

Jackson, M.D.[1] and Cassenti, D.N.[2]

[1]United States Army Research Laboratory, **RDRL-CII-T**, APG, MD, [2]United States Army Research Laboratory, **RDRL-HRF-D**, APG, MD

*corresp. author: marc.d.jackson6.ctr@mail.mil

The purpose of this study was to investigate decision making performance in a simulated network-enabled Mission Command task and to explore the relationship between the presentation of information and user decisions within these systems. The study was conducted online, using Amazons Mechanical Turk service. Participants were asked to play Shadow Force, a simulated game in which various assets with different capabilities are deployed to survey an area grid to identify hidden threats. Each asset provides information about whether an enemy target is, is not, or may be located in specific areas of the grid. We manipulated total rounds of asset deployment to represent cognitive workload (e.g. 3, 5, or 7). Each participant completed one of the three conditions. Our analysis revealed enemy targets were detected more frequently by participants with more rounds of assets in general. Additionally, there appeared to be a threshold where more rounds of feedback did not necessarily increase performance. Furthermore, we examined mode of information presentation preferences for participants and determined graphical representations may be more useful to optimize performance on Mission command tasks compared to text based reports. Lastly, we demonstrated which asset characteristics participants relied upon the most for feedback to reach a decision identifying target locations. We view this research as a starting point in addressing the factors that might contribute to performance in a simulated network-enabled Mission Command task and how best to present information to facilitate the decision making process.

Detection and characterization of chemical aerosol using laser trapping single-particle Raman spectroscopy

Kalume, A.[1], Beresnev, L.A.[1], Santarpia, J.L.[2] and Pan, Y.L[1]

[1]United States Army Research Laboratory, **RDRL-CIE-S**, Adelphi, MD, [2]Sandia National Laboratories, Albuquerque, NM

*corresp. author: aimable.kalume.ctr@mail.mil

Studying physical and chemical properties of aerosol particles in the ambient medium presents a unique tool in order to understand their dynamics, evolution and effects on our environment. In this perspective, a rapid detection and characterization of the presence of chemical agent aerosols in various complex atmospheric environments is an essential defense mission. Despite considerable efforts vowed to prevent the development, production, stockpiling and the use of chemical weapons, the World faces a constant sense of threat and fear, resulting from the increasing criminal and terrorist activities. Our research focuses on characterizing chemical agents and simulants as airborne aerosol particles. Recently, we developed a laser-trapping single-particle Raman spectrometer system, we trapped and characterized microdroplets of the VX nerve agent chemical simulant, diethyl phthalate. In additional to the good agreement with previous works and theoretical prediction, the uniqueness of the chemical fingerprint is enhanced by appearance of additional spectral features, related to the spherical nature of the microdroplets, namely stimulated Raman scattering and morphology-dependent whispering gallery modes. The resonance spectrum, resulting from the variations in the elastic scattered light as function of time, was compared to the simulation, based on Lorenz-Mie theory, to determine the microdroplet size at any given time. Due to its high efficiency in trapping and its precision in spectroscopic characterization, this method could be particularly suitable for detecting and characterizing hazardous substances such as chemical agents in complex atmospheric environments.

Synthesis and processing of nanocomposite ceramics for improved functionality of transparent materials

Ku, N.[1] *and Blair, V.*[1]

[1]United States Army Research Laboratory, **RDRL-WMM-E**, APG, MD

*corresp. author: nicholas.ku.ctr@mail.mil

Transparent polycrystalline ceramics are used in various applications, including laser hosts, infrared windows, and transparent armor. For such applications, superior optical, mechanical, and thermal properties of the material are required, yet the intrinsic properties of many traditional monolithic material systems are found lacking. Using nanocomposites in lieu of single phase, monolithic systems offers an engineering solution to this material problem. In this work, two dual-phase ceramic systems will be discussed for optical applications. First, the synthesis and processing of an Er:Y2O3 and MgO nanocomposite for use as a mid-infrared laser will be demonstrated. The advantage of adding MgO to the Er:Y2O3 lasing medium and creating a nanocomposite is the significant increase in thermal conductivity, allowing for improved laser gain. Also under investigation is a CaF2 and ZnS system for use in IR transparent missile domes. The use of a composite system will increase strength by reducing grain size of the product via grain pinning during sintering. For both systems, a wet chemical precipitation route is used for synthesis. The subsequent processing challenges involve with producing a sintered ceramic will also be discussed.

CANCELLED Effect of Zone Creation to Locally Control Microstructure in Powder Bed Fusion of 17-4 Stainless Steel

Kudzal, A.[1,2]*, Hofmeister, C.*[1]*, Galles, D.*[1]*, Hornbuckle, C.*[3]*, McWilliams, B.*[1] *and Liang, J.*[2]

[1]United States Army Research Laboratory, **RDRL-WMM-D**, APG, MD, [2]Worcester Polytechnic Institute, Worcester, MA, [3]United States Army Research Laboratory, **RDRL-WMM-F**, APG, MD

*corresp. author: andelle.d.kudzal.ctr@mail.mil

The microstructure and mechanical properties for powder bed fusion (PBF) additively manufactured 17-4 stainless steel parts are controllable by adjusting the laser processing parameters to locally control the thermal history. The powder bed energy density was manipulated such that the scan strategy was heterogeneous within a layer of the part to induce locally varying thermal histories, allowing for control of phase transformation kinetics and grain size. Microstructures were examined using optical microscopy, scanning electron microscopy, and x-ray diffraction and compared to reference samples produced using a homogeneous scan strategy. Finite element analysis was conducted of the PBF process to quantify the relative local heating and cooling rates and compared to experimental observations. Porosity was quantified using x-ray-microcomputed tomography to measure the effect of locally controlled regions on defect formation at zone boundaries. Locally changing the thermal history can create zones with decreased grain size and increased concentrations of retained austenite.

Multiscale Coarse-Graining with Effective Polarizabilities: A fully bottom-up approach

Lafond, P.G.[1] *and Izvekov, S.*[1]

[1]United States Army Research Laboratory, **RDRL-SEE-M**, Adelphi, MD

*corresp. author: patrick.g.lafond.ctr@mail.mil

Coarse-grain (CG) models offer a way to estimate the behavior of larger systems, for longer times than would be possible with full detail fine-grain calculations. For most atomistic simulations, CG models are constructed by eliminating electrostatic interactions, yet in many practical situations, such as energetic material (EM) sensitivity, the dielectric properties of a material are too important to ignore. In this work, we show that the instantaneous center of mass (CoM), charge, and dipole of clusters of atoms can be represented by charged dimers of CG particles. Using this simple representation, we derive a formal mapping of the microscopic coordinates to the dimer representation giving a fully bottom-up construction of CG force fields that statistically match not only the CoM, but for the first time, also match the leading terms of the multipole expansion. We first test the method on nitromethane showing its ability to work for a highly polar liquid EM. We find our CG nitromethane matches not only liquid structuring, but dipole statistics, and dipole structuring as well. We then test the method with poly(vinyl alcohol), where each repeat unit is represented by a single dimer. We find the derived polymer model matches monomer dipoles as well as intra-chain dipoles, allowing us to simulate composite materials interacting with external fields at the mesoscale. Lastly, we explore preliminary results of a CG solid RDX. We find the CG RDX model exactly matches the crystal structure and dipole statistics, meaning it will soon be possible to match the dielectric properties during simulations of shocked solid energetics. In the method presented here, unlike any previous bottom-up mapping, the atomistic particles are fractionally mapped to both sites in the dimer representation. Despite this difference, we show that our transformation is canonical, revealing a new family of previously unexplored CG methods.

Investigation of the origins of p-type behavior in annealed undoped $GaN_{1-x}Sb_x$ alloys

Llopis, A.[1]*, Segercrantz, N.*[2,3]*, Baumgartner, Y.*[3,4]*, Ting, M.*[4,5]*, Yu, K.M.*[6]*, Mao, S.S.*[5]*, Sarney, W.L.*[1]*, Svensson, S.P.*[1]*, Wraback, M.*[1] *and Walukiewicz, W.*[3]

[1]United States Army Research Laboratory, **RDRL-SEE-M**, Adelphi, MD, [2]Department of Applied Physics, Aalto University School of Science, Aalto, Espoo, Finland, [3]Materials Sciences Division, Lawrence Berkeley National Laboratory, Berkeley, CA, [4] Institute of Materials, Ecole Polytechnique Federale de Lausanne, 1015 Lausanne, Switzerland, [5]Mechanical Engineering Department, University of California, Berkeley, CA, [6]Department of Physics and Materials Science, City University of Hong Kong, Kowloon, Hong Kong

*corresp. author: llopis-jepsen.ctr@mail.mil

Photoelectrochemical (PEC) conversion of water into hydrogen gas has potential as a simple, ubiquitous, storable fuel source. By making use of a semiconductor whose valence and conduction band energies line up with the redox potential of water, it is possible to produce a photoelectrode for direct conversion of solar energy into hydrogen gas. GaNSb with concentrations of Sb between 5-7% is ideal for this application, as if fulfills the

energy level criterion, as well as being chemically resistant and stable in water. Preliminary work here at ARL on these alloys has demonstrated $GaN_{1-x}Sb_x$ with p-type nature, which is in-and-of-itself of great value due to the difficulty of producing p-type GaN for development of optoelectronic devices based on III-V nitride semiconductors. Results have shown post-annealing hole concentrations almost an order of magnitude higher than those produced with Mg-doped GaN, the current standard for doping GaN. In both cases it is important to understand the carrier transport processes and recombination pathways within the material. In order to investigate the carrier dynamics within these GaNSb alloys, we have performed time-resolved differential reflection and transmission measurements using the pump-probe method with resolution on the order of 100 fs. Further measurements on the same samples were performed post-annealing to investigate the origins of the p-type behavior and changes in the carrier dynamics. We present these results and discuss their relevance and impact on the use of these alloys for PEC water splitting and as p-type material for use in bipolar junction optoelectronic devices.

Femtosecond Laser Machining of Micro-tensile Specimens for High Throughput Mechanical Testing

Magagnosc, D.J.[1], Ligda, J.P.[2], Sano, T.[2] and Schuster, B.E.[1]

[1]United States Army Research Laboratory, **RDRL-WML-H**, APG, MD, [2]United States Army Research Laboratory, **RDRL-WMM-F**, APG, MD

*corresp. author: daniel.j.magagnosc.ctr@mail.mil

Recently, a variety of techniques for fabricating microscale specimens for mechanical testing have been developed. However, many of these techniques are limited by material compatibility, specimen sizes, low throughput, or microstructural damage. In contrast, the advent of femtosecond laser systems offer opportunities to circumvent many of these challenges. Here we demonstrate the use of a femtosecond laser milling system to rapidly fabricate micro-tensile specimens across a range of critical dimensions, from 10s to 100s of microns. By incorporating the laser milling system into a custom micromechanical testing apparatus, we are able to achieve high throughput investigations of mechanical properties at the microscale. These capabilities are demonstrated on metal and ceramic materials.

Chemical Energy Dense Production using Microporous and Meso-Microporous Solid Acid Catalysts: Zeolites

Mahoney, L.[1], Emdadi, L.[1], Dunbar, Z.[1], Tran, D.[1] and Lee, I.[1]

[1]United States Army Research Laboratory, **RDRL-SED-E**, Adelphi, MD

*corresp. author: luther.j.mahoney.ctr@mail.mil

Our motivation for developing energy dense chemical storage include the ability to use energy on demand when needed for extended time periods. The U. S. Army has a seven day mission challenge and beyond. This work addresses the needed long-term portable energy demand applications with creating higher chemical energy storage media. The chemical process involves taking waste food or similar waste chemical composition exposed to food-grade bacteria with resulting low energy fragments. The food fragment are converted to approximately 20% aqueous ethanol (5 MJ/kg). After subjecting the 20% ethanol to ethene gas with water formed, then, the ethene is subjected to an optimized reaction conditions: 8 h reaction period; 0.41 h-1 (WHSV); 400 °C reaction temperature; and atmospheric pressure. The micro-gas-chromatography (micro-GC) results show we can produced up to 70% liquid products comprised of energy dense aromatic compounds in the range of kerosene. The energy content of the liquid products was 40 MJ/kg, which is similar to gasoline. The liquid product yield range was from 0.8 g to 1.4 g with coke fouling controlled by the pore geometry and metal dopant used. This research endeavor paves the way to carefully evaluate pore geometry with 2% (weight percent) zinc, and we are in the process of converting aqueous ethanol to liquid range hydrocarbons in two consecutive reactions. Our experimental approach can be scaled for portable on-demand use for soldiers and related applications in the endeavor to meet the 7 day U.S. Army mission challenge.

Extraction of Metamaterial Constitutive Parameters Using the First-Principle Homogenization Theory

Nguyen, Q.[1] and Zaghloul, A.I.[1]

[1]United States Army Research Laboratory, **RDRL-SER-M**, Adelphi, MD

*corresp. author: 93nguyen@cua.edu

Metamaterials have received considerable attention in the electromagnetic community due to novel physics and engineering properties such as simultaneously negative permittivity, ε, and permeability, μ. Being able to determine correctly the permittivity and permeability is essential to characterize metamaterials.

Most common techniques in the retrieval process are based on the Nicolson-Ross-Weir (NRW) equations. The procedure is as follows. The effective refractive index n, and impedance, z, are first obtained by using S scattering parameters calculated from a wave incident normally on a metamaterial sample. Then the permittivity, ε, and permeability, μ are determined by $\mu = nz$ and $\varepsilon = n/z$ respectively.

However, the NRW equations assume that the tangential electric and magnetic field are continuous across the interface. This assumption may not be able to capture the surface perturbation effects. Thus, the constitutive parameters retrieved by the NRW approaches for metamaterial medium may not satisfy the conventional causality and passivity conditions for permittivity and permeability, resulting in the wrong sign of the imaginary parts and negative slopes versus frequency. This unexpected effect is also known as "resonant/anti-resonant coupling".

The first-principle homogenization theory (FPHT), proposed by Andrea Alu, can accurately describe the response of metamaterial. It utilizes the polarizabilities of a single resonant scatter to extract the bulk effective parameter of a 3D periodic scatter array. In this work, we implement the FPHT to calculate the effective permittivity and permeability response of metamaterial. The split-ring resonator (SRR) configuration is chosen as the test case to validate the constitutive effective parameters using FPHT against the effective parameters obtained by NRW.

Development of a Hybrid Vehicle Capable of Performing Advanced Maneuvers with On-board Sensing

Nogar, S.[1]

[1]United States Army Research Laboratory, **RDRL-VTA**, APG, MD

*corresp. author: stephen.m.nogar.ctr@mail.mil

There is a strong need to develop small scale (< 30 cm) vehicles that can achieve long endurance, maintain flight agility, and fly in GPS denied environments. Hybrid vehicles, i.e. a vehicle that can hover and transition to forward flight, offer both efficiency and agility. This project develops a hybrid vehicle using a tailsitter design and novel dual tilting rotors. Transition between hover and forward flight is achieved by rotating the body 90 degrees and control authority is provided by only the tilting rotors in a minimally actuated design. The unique vehicle configuration requires novel control strategies that account for the large body rotations and are able to perform controlled transition from hover to forward flight. A vehicle prototype has been developed that implements the control strategy on-board and is able to demonstrate transition. Current and future work are focused on increasing agility, perception capabilities and autonomy.

Exploring Kevlar® Fiber Processing-Internal Structure-Property Relationships Through a Novel FIB Notch Technique

Roenbeck, M.R.[1], *Sandoz-Rosado, E.J.*[2], *Cline, J.*[3], *Wu, V.*[3], *Moy, P.*[3], *Afshari, M.*[4], *Reichert, D.*[4], *Lustig, S.R.*[5] *and Strawhecker, K.E.*[1]

[1]United States Army Research Laboratory, **RDRL-WMM-G**, APG, MD, [2]United States Army Research Laboratory, **RDRL-WMM-A**, APG, MD, [3]United States Army Research Laboratory, **RDRL-WMM**B, APG, MD, [4]E.I. du Pont de Nemours and Company, DuPont Protection Solutions, Richmond, VA, [5]Department of Chemical Engineering, Northeastern University, Boston, MA

*corresp. author: michael.r.roenbeck.ctr@mail.mil

Advancements in processing techniques have facilitated the development of a n expansive set of distinct high-performance DuPont^{TM} Kevlar®fibers . Characterizing fibers interior structures is vital for linking processing conditions with resulting structures and mechanical properties . However, the complex, multiscale structural motifs throughout Kevlar®fibers have introduced significant difficulties in developing direct, comprehensive understanding of these structures. Here we report detailed investigations of processing-internal structure-property relationships among four distinct classes of Kevlar®fibers (K119, K29, KM2+, and K49). We employ a novel focused ion beam (FIB) notch technique to obtain pristine interior fiber planes and measure morphology and transverse stiffness across these surfaces via multifrequency atomic force microscopy (AFM) maps. Combining multiscale AFM observations with tensile tests of single fibers drawn from the same tows, we uncover distinct interior structural phenomena that provided clear footprints of processing effects and corresponding impacts on mechanical behavior. Most notably, we uncover alternating stiffness bands that are especially apparent in low -modulus, non- heat -treated fibers, revealing a unique manifestation of internal structural variations that helps explain the observed trends in material responses.

Electrolytes for Next Generation Lithium Batteries

Schroeder, M.[1], *Alvarado, J.*[2], *Gobrogge, E.*[1], *Ding, M.*[1], *Borodin, O.*[1] *and Xu, K.*[1]

[1]United States Army Research Laboratory, **RDRL-SED-C**, Adelphi, MD, [2]Materials Science and Engineering University of California: San Diego, CA

*corresp. author: marshall.a.schroeder.ctr@mail.mil

Harnessing the enhanced energy and power metrics offered by "5V-class" lithium-ion electrode chemistries relies on development of more robust electrolytes with expanded voltage and temperature stability windows. As a part of this effort, we have explored the promise of a variety of electrolyte solvents and additives, focusing on systems that promote new levels of oxida tive stability (generally >5.0V vs. Li/Li+ compared to ~ 4.3V for conventional electrolytes), safety, and compatibility wit h next generation electrode systems. Unfortunately, due to shortcomings such as high melting points, viscosity, or the inability to independently form a stable solid electrolyte interphase (SEI), practical implementation of many of these materials is gener ally limited to use as minority co-solvents in more conventional electrolyte systems. By exploring the effects of solvation, concentration, and salt chemistry on electrolyte performance, our group has had a recent breakthrough, characterizing the formation of a stable SEI which enables full utilization of the graphite electrode for the first time in an "EC-free" electrolyte with a sulfone as the primary solvent. In high voltage full cells, the oxidative stability of the system is confirmed by voltammetry an d galvanostatic cycling measurements. Anode and cathode surface chemistry is explored extensively with XPS, and will be coupled with computational calculations to propose a mechanism for the formation and operation of both electrode/electrolyte interphases.

Microstructural study in B$_4$C-SiC ceramic-ceramic matrix composites

Shoulders, W.T.[1], *Behler, K.D.*[1,2], *Vargas-Gonzalez, L.*[1]

[1]United States Army Research Laboratory, **RDRL-WMM-E**, APG, MD, [2]SURVICE Engineering, Belcamp MD

*corresp. author: william.shoulders7.ctr@mail.mil

In the search for body armors improving on the weight of SiC and ballistic performance of B$_4$C, experimental compositions have moved increasingly towards engineered structures at length scales ranging from the atomic scale (defects and grain boundaries) all the way to the macro-scale (layering, segmenting). Perhaps one of the most popular trends in industrial experimental armor blends is modification at the micro-structure scale. This work draws on early stage microstructural studies in order to provide better understanding of both processing-structure relationships and structure-performance relationships. The first phase of this project covers fabrication of a series of B$_4$C-SiC composites having a systematic compositional variation between the monolithic ceramics in increments of 10 wt%. Microstructures are controlled by the agglomeration and sieving of component powders in-house. The samples are consolidated to near-theoretical density by hot-pressing at 1950 °C. Full structural and chemical characterization is performed using optical microscopy, scanning election microscopy (SEM), x-ray fluorescence (XRF), x-ray diffraction (XRD), and micro-Raman spectroscopy. Hardness is determined by the

static indentation method using a Knoop indenter. Trends in harness and crack morphology are tracked as a function of chemistry and structure. To explore the role of crack arrest and deflection by stress fields, an analysis of the residual stress is performed locally using micro-Raman spectroscopy.

DFT Calculations of Arg and Lys on Au(111) to Probe the Effects of Amino Acid Conformation and Dispersion on Binding

Small, M.C.[1], *Terrell, J.L.*[2], *Sarkes, D.A.*[2], *Jahnke, J.*[2], *Stratis-Cullum, D.N.*[2] *and Hurley, M.M.*[1]

[1]United States Army Research Laboratory, **RDRL-SEE-B**, APG, MD, [2]United States Army Research Laboratory, **RDRL-SEE-B**, Adelphi, MD

*corresp. author: meagan.c.small.ctr@mail.mil

Biomolecular-inorganic hybrid materials have many potential applications in medicine, electronics, and nanotechnology. Of great interest is designing peptides that have predictable and controllable binding to inorganic surfaces, which requires a detailed understanding of the binding interactions between the amino acids and inorganic surface. Computational models have provided key insight into the underlying intermolecular interactions in such systems, including probing the effects of dispersion and hydration. However, owing to limited computational resources, these studies are often performed using periodic models where care must be taken to understand the effects of model size and periodicity, as well as any possible additional limitations in the method. In this study, we have performed quantum mechanical (QM) calculations at the DFT level of theory for the side chains of Arg and Lys on an Au(111) slab that is of sufficient size to mitigate periodicity-based artifacts. Furthermore, multiple orientations of the amino acid on the slab have been calculated with and without dispersion to compare the effects of conformation and dispersion on binding. The results show that most favorable residue orientations differ significantly when dispersion is explicitly included. For Arg, the guanidinium group is oriented perpendicularly to the surface when dispersion is not included and planar when dispersion is added. Similarly, the alkyl chain of Lys lays flat along the surface of the slab when dispersion is included, yet tends to be at a diagonal with the amine closest to the surface in the absence of dispersion. Lastly, the results will be discussed in the context of existing computational and experimental data for the binding of amino acids on Au(111), as well as the potential for using this data to refine existing bio-inorganic force fields (FFs) and guide future model development of peptides on inorganic surfaces.

Recent progress in acoustic wireless power transfer: Phased array focusing and improved receiver design

Tseng, V.F.G.[1], *Bedair, S.S.*[1] *and Lazarus, N.*[1]

[1]United States Army Research Laboratory, **RDRL-SED-E**, Adelphi, MD

*corresp. author: victorfarm-guoo.tseng.ctr@mail.mil

Wireless power transfer (WPT) through acoustic/ultrasonic waves can achieve higher power transfer efficiencies than inductive coupling when the distance is above several times the transducer size. Acoustic WPT can also transfer power through various mediums including air, water, and conductive material. In order to further increase the performance of acoustic WPT, we have demonstrated the feasibility of phased array power focusing and beaming, and also investigated the design of a receiver array to improve the receiver efficiency and power combining. This presentation summarizes the current progress we have achieved. With a 40 kHz, 37 element, 7 cm total diameter phased array transmitter, acoustic focusing could be used in the near field region to increase the power transfer efficiency by 2.6 times when compared to an equivalent case with no acoustic focusing. Beam steering could also be used to actively adjust the focal point location. The experimental results were shown to closely match numerical modeling results, predicting that the efficiency can be further doubled by increasing the number of array elements. By further substituting for a 7element receiver array design, another 4.25 times increase in efficiency can be achieved when compared to only using the receiver center transducer. An inductive WPT system with equivalent size was also built and tested for comparison, showing that the acoustic WPT system can achieve higher efficiencies than the inductive WPT system when the transmit-to-receive distance is above 5 cm.

Measuring tip-sample thermal conductance mechanisms for robust quantitative nanoscale thermal analysis via scanning thermal microscopy

Wilson, A.A.[1]

[1]United States Army Research Laboratory, **RDRL-SED-E**, Adelphi, MD

*corresp. author: adam.a.wilson6.ctr@mail.mil

Recently, thermal transport and energy conversion phenomena in nanostructures have been theorized to provide a means for high-efficiency, transformative solid-state thermal energy conversion technologies, such as nanobulk thermoelectrics [1], and thermoelectrics using nanowires [2] or nanotubes [3]. However, experimental validation of the behavior of these local transport phenomena is lacking because state of the art thermal characterization techniques rely on probing mechanisms which are limited laterally to the microscale or larger. Scanning thermal microscopy provides ultra-high resolution (10s nm), but to-date has been generally limited to qualitative or relative measurements, and has been regarded as unreliable for thermal conductivity measurement [4]. This work reports a strategy combining passive-mode and active-mode scanning thermal microscopy to calibrate the probes temperature response for robust quantitative sample temperature and thermal conductivity measurement. The same test structure used to calibrate the tip is used to measure the gap thermal conductance, thermal conductance across the water meniscus, and solid-solid thermal conductance. De-coupling the overall tip-to-sample thermal conductance into these three mechanisms allows for ultra-high resolution, non-destructive interrogation of thermal, hydrostatic, and mechanical properties of this test sample with nanoscale resolution.

Development of a UHMWPE Thermoforming Process Model

Yeager, M.[1] and Bogetti, T.[1]

[1]United States Army Research Laboratory, **RDRL-WMM-B**, APG, MD

*corresp. author: michael.yeager11.ctr@mail.mil

Ultra-high molecular weight polyethylene (UHMWPE) has shown potential for enhancing the ballistic performance of combat helmets. UHMWPE helmets are manufactured in a complex multi-step thermoforming process comprised of preforming and consolidation stages. Although experimental results have demonstrated the tremendous influence that processing conditions have on ballistic performance, manufacturing parameters are still developed utilizing a expensive trial and error approach, both in cost and time. A comprehensive virtual manufacturing framework is being developed to predict material deformation and fiber reorientation during the thermoforming process. Preforming, the first step in the process, involves a punch pressing UHMWPE sheets through a female die plate. A binder plate is utilized to supply pressure between the sheets and die plate, which increases frictional forces to prevent wrinkle formation in the UHMWPE sheets. This poster presents a single curvature preforming model, which isolates shear and friction from the complex wrinkling process. It will be employed to study the influence of punch rate, binder pressure, and friction on the preforming deformation mechanisms present in UHMWPE sheets. In the future, it will be extended to a double curvature model to predict the preforming of hemispheres.
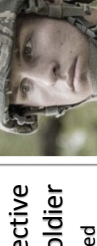
Appendix B. Contributed Posters Presented at the 2ⁿᵈ Postdoc Research Day

Electrochemical Performance of Lithium-ion Capacitors Evaluated under High Temperature and High Voltage Stress

Jonathan Boltersdorf,[†] Samuel A. Delp,[†] Jin Yan,[β,§] Ben Cao,[β] Jim P. Zheng,[§] T. Richard Jow,[†] and Jeffrey A. Read[†]

[†] United States Army Research Laboratory, RDRL–SED-C, Adelphi, MD 20783-1138, USA
[β] General Capacitor LLC & INTL., INC. Tallahassee, FL 32304, USA,
[§] Department of Electrical and Computer Engineering, Florida A&M University-Florida State University, Tallahassee, FL 32310-6046, USA

Background and Motivation

low power, high energy

Li-Ion Batteries
Li-ion transport & intercalation Faradaic redox reactions

med. power, med. energy

Supercapacitor (EDLC)
Electrochem. Double Layer Capacitance Ion adsorption–desorption

high power, mod. energy

Hybrid Li-ion Capacitors
Li-ion transport & intercalation and EDLC ion adsorption–desorption

Graphite or HC   AC or LIB cathode/AC

Arandon, V. et al. Chem. Rev. 2014, 114, 11619-11635.
Xu, K.Chem. Rev. 2014, 114, 11503-11618.
Liu, J. Nat. Nanotech. 2014, 9, 739-741.

Hybrid Li-ion Capacitors (LICs):
• Higher energy density than EDLCs
• Higher power density than LIBs
• High reliability/cycle life, similar to EDLCs
• High cell capacity (i.e., large anode capacity)
• Faradaic and Electric double-layer energy
• Safe (less susceptible to thermal runaway)
• Operating temperatures from -20 to 65 °C
• Low self-discharge (5% loss over 3 months)

high power, low energy

Capacitor
Electrical Capacitance Conductive parallel plates

AC = Activated Carbon; HC = Hard Carbon

Research Objectives

• Develop new hybrid electrochemical devices that incorporate the advantages of the Li-ion battery and the electrochemical capacitor, while improving on their inherent defects
• Operation of LIC power source in high stress conditions (e.g., high temperature, rate, voltage, etc.) to simulate extreme environments
• Provide rapid charge capability to meet high power density requirements
• Identify optimal conditions for LIC energy devices for i) LIC cell design, ii) electrolyte and additive development, and iii) rigorous performance testing

Potential Applications of LICs

Challenges

• Prelithiation process of the carbon-based negative electrode (anode)
• Deterioration and gassing of the electrolyte during formation and cycling of LICs
• Stability of carbonaceous active electrode materials, safe operational limits of the electrolyte, and the configuration of the electrodes for hybrid cell design
• Evaluation of the rate performance (1C to 10C rate), temperature performance (25 to 65 °C), voltage stability window (2.2 V to 3.8–5.0 V), and cycle life under high stress conditions

LIC Cell Design and Formation

Figure 1. Lithium-ion capacitor (a) 3-layer cell design with 2 single-sided AC cathodes and a double-sided HC anode. The (b) pre-lithiation of the HC anode using lithium-metal strips is shown.

• Pre-lithiation of Carbon-based Anodes: lithium metal is used to introduce lithium-ions into the system by electrochemical/chemical reaction with the anode
• Pre-lithiation of the anode is an important step typically obtained via:
  → ex-situ electrochemical lithiation by using a separate Li half cell, which increases the device's cost and process complexity due to extra procedure and handling of electrolyte-wetted anode
  → in-situ electrochemical lithiation by embedding a Li foil as the third electrode into LIC, which reduces energy density and increases the device's cost due to extra cell components
  → Chemical lithiation by reacting with SLMP or a Li foil

Electrolyte and Additive Formulation

Lithium Salt   Cyclic Carbonates   Linear Carbonates
Additives

Base Electrolytes:
1 M LiPF6 EC:DMC
1 M LiPF6 FEC:DMC
1.2 M LiPF6 3EC:7EMC
Ratios – 1:1 and 3:7

Figure 2. Electrolyte and additive components used in this study.

• Electrolyte is critical for optimizing performance and long-term stability
  • SEI formation due to decomposition of electrolytes/additives on electrodes
  • Additives improve electrode stability, extending cell cycle life
  • Anode additives reduce at higher potentials than carbonate electrolytes
  • Cathode additives oxidize at lower potentials than carbonate electrolytes

Rate Performance of Three-Layer LICs

Figure 3. Comparison of the specific energy and power density obtained from the rate performance tests of the three-layer LIC cells at discharge rates ranging from 1C to 10C using (a) base electrolytes with different EC to DMC/EMC solvent ratios, (b). EC:DMC and 3EC:7EMC based electrolytes with various additives, and (c) EC:DMC electrolyte with different TMSP additive content.

Long-Term Performance Tests of Three-Layer LICs

Figure 4. Cycle life performance at room temperature shown by alternating float at 3.8 V and cycling of the three-layer LIC cells using various electrolytes with additives. The (a) specific discharge capacity and (b) coulombic efficiency tests are plotted for a 10C charge/discharge rate.

Critical Performance Tests at High Stress Conditions of Three-Layer Lithium-ion Capacitors

Figure 5. Room temperature float-cycle of LIC cells at increasing upper cut-off potentials using the EC:DMC and 3EC:7EMC based electrolytes with various additives. The (a) specific discharge capacity and (b) coulombic efficiency tests are plotted for 200 mV increments at a 10C charge/discharge rate.

Figure 6. High temperature (65 °C) float at 3.8 V and 25 °C cycling (10C rate) of LIC cells using (a) EC:DMC and 3EC:7EMC based electrolytes with VC and TMSP additives, and (b) EC:DMC electrolyte with different TMSP additive content, as well as electrolytes with different EC to DMC/EMC solvent ratios.

Accomplishments / Future Direction

• The VC and TMSP additives were found to be essential to the improved rate performance of the LIC cells at higher discharge rates
• The LIC cells exhibited long-term float-cycle life performance at 25 °C (i.e., 1200+ hours at 3.8 V and 500+ cycles) with high capacity retention and stable coulombic efficiencies
• At 4.0 V, the EC:DMC electrolyte with 1% VC and 1% TMSP additives showed high capacity retention (~97.9% and ~116%) compared to EC:DMC without additives
• The LICs show long cycle life performance in the float at 65 °C and cycle at 25 °C tests

• Identify role of TMSP additive in LIC cells
• Develop and test hybrid battery/AC cathodes in order to improve flexible rate capabilities
• Identify ideal battery:AC ratio and electrolyte formulation stable at high stress conditions

Comparison of the in-plane shear behavior of UHMWPE fiber and highly oriented film composites

Julia Cline, Travis Bogetti, Bryan Love

Weapon and Materials Research Directorate, MMSD, RDRL-WMM-B

Research Objective

- Evaluating emerging candidate materials for lightweight protective systems for the dismounted soldier
  - Highly oriented solid state extruded polyethylene (SSE-PE) film
- Understand the underlying mechanisms behind improved back-face deflection performance of SSE-PE composites
  - Increased in-plane shear stiffness over traditional gel spun UHMWPE fiber based composites
  - In-plane stiffness may change the mechanisms during a ballistic event and engage more material in dissipating impact energy

Analysis

- Large deformation and significant fiber rotation
- Quantify fiber rotation angles using continuum mechanics approach

$$F = \begin{bmatrix} \lambda & 0 & 0 \\ 0 & \alpha & 0 \\ 0 & 0 & \beta \end{bmatrix} \qquad E = \frac{1}{2}(C - I) = \frac{1}{2}(F^T F - I) \qquad \theta = \frac{1}{2}cos^{-1}\left(\frac{(\lambda^2 - \alpha^2)}{(\lambda^2 + \alpha^2)}\right)$$

- Strain energy density calculations used to determine matrix and fiber stress strain response
- Fibers do not deform significantly
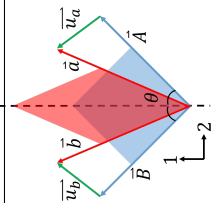
Technical Approach

- Compare the in-plane shear response of SSE-PE (Tensylon® 30A) to well-studied UHMWPE fiber based system (Spectra Shield® SR 3136)
- Tensile tests of thin [±45°] laminate specimens
  - DIC used to measure in-plane deformation as a function of axial load
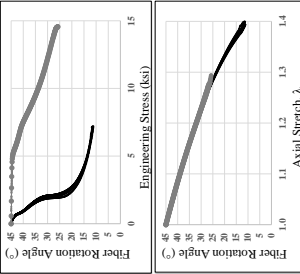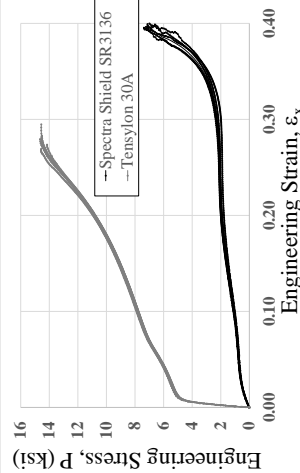
Conclusions / Future Direction

- Fiber rotation is a primary deformation mechanism that needs to be accounted for in analysis
- Perform ballistic testing (V_{50} and BFD) on laminates to assess influence of fiber rotation on ballistic performance
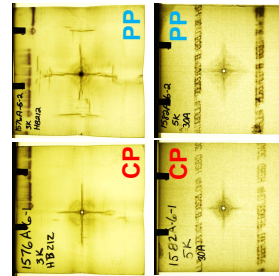
Predicting Human Interactions with an Automation

Kim Drnec, Evan Carter, Jason S. Metcalfe, Justin Estepp, Greg Gremillion, Amar Marathe

Warfighter Challenge: How to improve human agent team performance so that it can reach anticipated levels necessary for mission success?

Background

Trust in automation has long been considered to be the mediating factor between automation capability and appropriate use. The interaction behavior, or automation use is the result of a decision we term trust-based decisions.

Proposed Solution

Prediction of the trust-based decision from various environmental and psychophysiological features, allowing mitigation of inappropriate trust-based decisions in real time thus improving human agent team performance

Hypothesis

A classifier will be able to use environmental and psychophysiological features to predict how and when a participant will interact with the automation

Feature Source

Features derived from a simulated driving study aimed at understanding trust-based decisions (Figures 1 & 2)

Methods

- 365 Features
  - Psychophysiological (EEG spectral power)
  - Environmental (Course features)
- Hierarchical Discriminant Component Analysis classifier (HDCA)
- Recursive selection
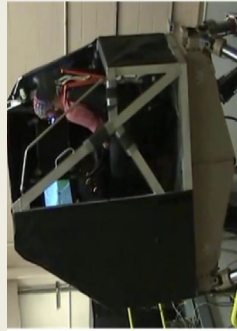- Artificial trial generation

Figure 1. Ride Motion Simulator at TARDEC

Figure 2. Participant view of driving scenario

Final Features

Hand-offs
- Perturbation type
- Inverse time to contact
- Beta power (F8
- Gamma power(P, F7, C5)
- Delta power(F5, Af4)
- Perturbation direction
- Frontal theta asymmetry

Take-overs
- Perturbation type
- Inverse time to contact
- Alpha power(F1, Af4)
- Delta power (Cp2)
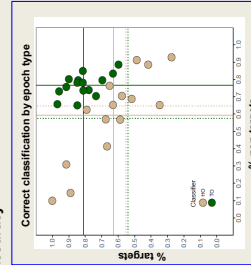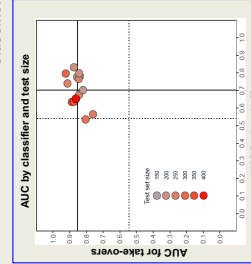- hEOG variance
- Gamma power (Iz)
- Beta power (Cp2)

Hand-offs = operator gives control to the automation.
Take-overs = operator takes control from the automation

Results

Classifier methods

Artificial trial generation

Recursive feature selection
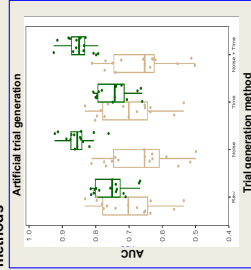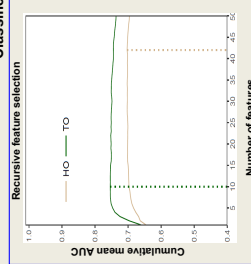
Classifier accuracy

Correct classification by epoch type

AUC by classifier and test size

Conclusions

- HDCA classification can predict a change of control authority 3 seconds before it happens with an AUC above chance
- Take-overs are better predicted than hand offs
- Artificial trial generation significantly increases prediction accuracy

The Nation's Premier Laboratory for Land Forces

Approved for Public Release. Distribution Unlimited

Determination of Partial Ordering in Pseudomorphic AlGaN Films Grown on AlN Single Crystals

Applications to Three-beam X-ray Multiple Diffraction Characterization on III-Nitride Heterostructures

M.B. Graziano, R.P. Tompkins, and K.A. Jones – Sensors and Electron Devices Directorate, Army Research Laboratory, 2800 Powder Mill Rd., Adelphi MD 20783

Three-beam X-ray Multiple Diffraction (XRMD)

- Occurs when an x-ray beam impinges on a single crystal in such a way that Bragg's law is satisfied for several crystal planes
- Observed in Renninger scans (RS), in which the diffractometer is set to a forbidden or weak symmetric reflection, i.e. (0001) for wurtzite
- The sample is rotated along its azimuth (φ), allowing the x-ray beam to be diffracted by a primary and secondary set of planes at select orientations, resulting in multiple diffraction peaks (MPs) in RSs
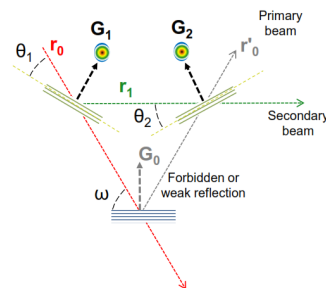
Partial Ordering of $Al_xGa_{1-x}N$ Ternary Alloy

- **Al** and **Ga** cations are distributed within the unit cell, occupying the (001) and $\left(\frac{1}{3},\frac{2}{3},\frac{1}{2}\right)$ sublattice sites, referred to A and B, respectively
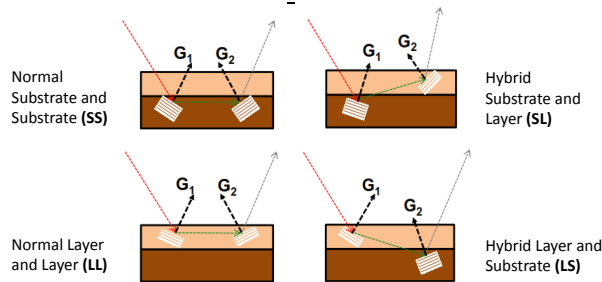- The structure factor for an $(hkil)$ $Al_xGa_{1-x}N$ Bragg peak is given by:

$$F_{(hkil)} = f_A + f_B e^{2\pi i\left[\frac{h+2k}{3}+\frac{l}{2}\right]} + f_N e^{2\pi i\left[\frac{h+2k}{3}+\frac{l}{2}\right]},$$
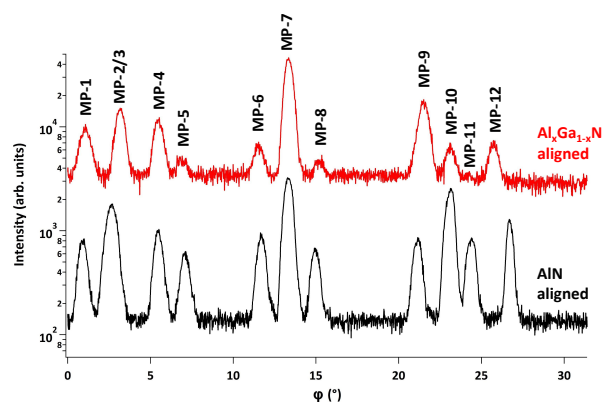
where f_A and f_B are the average atomic structure factors of the cation atoms in A and B sublattice sites and f_N is the atomic scattering structure factor of the **N** atoms

- For l = odd and h + $2k$ = $3n$, $F_{(hkil)} = 0$ if there is a **random** arrangement of cation species; otherwise, if there is **atomic ordering**, then $F_{(hkil)} \neq 0$, and these reflections become **visible** in x-ray diffraction measurements.

## Possible XRMD Paths in $Al_xGa_{1-x}N$/AlN Heterostructures

Normal Substrate and Substrate **(SS)**

Hybrid Substrate and Layer **(SL)**

Normal Layer and Layer **(LL)**

Hybrid Layer and Substrate **(LS)**

RS Diagrams for (0001) $Al_xGa_{1-x}N$/AlN

$Al_xGa_{1-x}N$ aligned

AlN aligned

| Number	XRMD Reflection Combination	φ-position (°) $Al_xGa_{1-x}N$	φ-position (°) AlN	Possible XRMD Path (Based on Absolute Intensity)
MP-1	$(3\bar{2}\bar{1}0)/(\bar{3}211)$	0.95	0.81	**Normal LL and SS**
MP-2/3	$(3\bar{1}\bar{2}2)/(\bar{3}123)$ $(1\bar{1}01)/(\bar{1}102)*$	3.05*	2.55*	**Normal LL and SS**
MP-4	$(02\bar{2}1)/(0\bar{2}20)$	5.39	5.35	**Normal LL and SS**
MP-5	--	**6.80**	**6.99**	**Hybrid SL or LS?**
MP-6	$(02\bar{2}2)/(0\bar{2}2\bar{1})$	11.41	11.59	**Normal LL and SS**
MP-7	$(1\bar{1}00)/(\bar{1}100)$	13.22	13.23	**Normal LL and SS**
MP-8	--	**15.07**	**14.84**	**Hybrid SL or LS?**
MP-9	$(3\bar{1}\bar{2}0)/(\bar{3}121)$	21.39	21.06	**Normal LL and SS**
MP-10	$(01\bar{1}3)/(0\bar{1}1\bar{2})$	23.01	23.05	**Normal LL and SS**
MP-11	$(12\bar{3}3)/(\bar{1}\bar{2}3\bar{2})$	24.16	24.30	**Normal LL and SS**
MP-12	$(02\bar{2}3)/(0\bar{2}2\bar{2})$	25.62	26.59	**Normal LL and SS**

- **First Time**: (0001)-oriented RSs on high quality $Al_xGa_{1-x}N$/AlN materials that resolve **twelve** three-beam MPs within a 30° sample rotation (φ=0° corresponds to the azimuthal direction $[10\bar{1}0]$)
- No mirror-reflected 60° periodicity, due to the **AlN wafer curvature** and **$Al_xGa_{1-x}N$ crystallographic tilt**, elastic mechanisms induced by the unrelieved residual compressive strain in the alloy films
- Theoretical calculations do not predict angular positions for **MP-5** and **MP-8**, suspected hybrid MPs that strongly depend on the substrate Bragg peak alignment

Observation of Pure (0001) $Al_xGa_{1-x}N$ Reflection

210 nm $Al_{0.51}Ga_{49}N$ Pseudomorphic

810 nm $Al_{0.71}Ga_{29}N$ Pseudomorphic
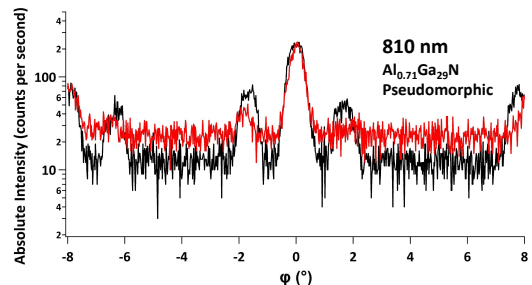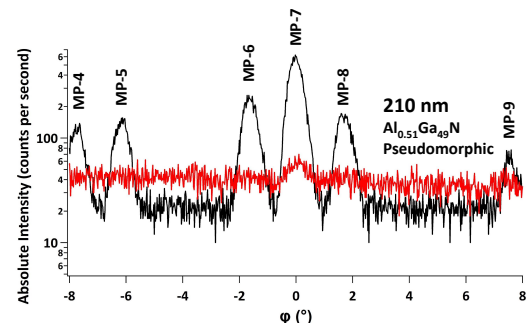
- **Diffraction from $Al_xGa_{1-x}N$ (0001) Bragg peak**: **change in absolute diffracted intensity**, as observed by Kyutt et al. **[1]**
- Intensity of (0001) $Al_xGa_{1-x}N$ pure reflection and MPs is much weaker than those reported in literature due to much smaller film thicknesses

Strain-induced or Film Growth Related?

210 nm $Al_{0.51}Ga_{49}N$ RMS = 0.083 nm

810 nm $Al_{0.71}Ga_{29}N$ RMS = 0.299 nm
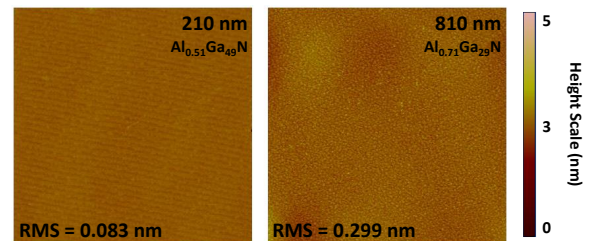
- Compositional inhomogeneity in $Al_xGa_{1-x}N$ alloys has been previously linked to adatom surface kinetics during growth, where improper growth conditions can lead to unequal incorporation of Al and Ga species in the film, resulting in step-bunched surfaces
- **The films investigated in this study did not possess this characteristic morphology**
- As such, the visibility of pure (0001) diffraction is attributed to preferential self-organization of Al and Ga atoms within the unit cell **in response to the built-in residual compressive strain energy in the ternary alloy film**

[1] R.N. Kyutt and S.V. Ivanov, Physics of the Solid State **56**, 2390 (2014)

Finite Element Analysis of Protective Footwear

Carolyn E Hampton, Michael Kleinberger
WMRD, Protection Division, Soldier Protection Sciences Branch

Research Objective

- **Background**
  - 82% of Army injuries attributed to explosive sources (Belmont 2013)
  - Majority of medical discharges due to extremity injury (Masini 2009)
  - Lower extremity fractures represent 18.5% of injuries (Belmont 2013)

- **Goals**
  - Create a finite element human body model from CT scan data
  - Combine data from simulations and experiments to identify injury mechanisms
  - Support development of novel protective equipment to reduce and mitigate Army injuries
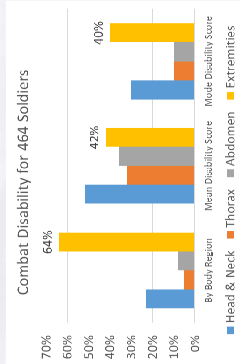
Fig 1. Injuries by frequency, mean severity, and mode severity (Masini 2009)

Challenges

- Discretizing complex biological structures into high-quality finite element meshes
- Supporting multiple solvers
- Adapting low-speed material data for use in rate-sensitive, viscous biomaterial models
- Capturing microscale level failure events within a continuum-based approach

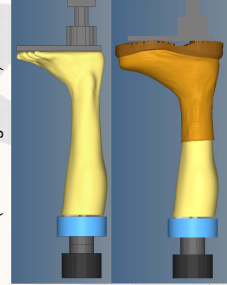Fig 2. Pendulum experiment (Gallenberger 2013)

Fig 3. Finite element leg models

Technical Approach

- Simulate paired booted/unbooted lower leg pendulum experiments at 5, 7, and 10 m/s (Gallenberger 2013)

- Compare simulation to experiment
  - Simulated peak tibia forces were +7.6% on average
  - Curve correlations were good (0.86 out of 1)
  - Stress concentrations correlate to fracture locations

- Assess geometry effects on force
  - Low arch height increased peak force +11.4%
  - Thicker heel pad reduced peak force -8.4%

- Quantify boot protective capability
  - Boots in experiment reduced peak force by 39.8%
  - Simulated boots reduced peak force by 33.5%
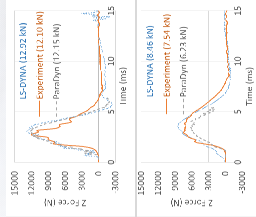
Fig 4 Tibia force, 10 m/s
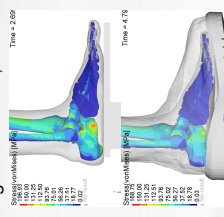
Fig 5. Stress contours, 7 m/s

Accomplishments / Future Direction

- Accomplishments
  - Finite element simulation matches experiments
  - Demonstrated boots mitigate 1/3 of peak force

- Future direction
  - Assess protective gear for additional body regions
  - Leverage scaling and posturing techniques
  - Provide assessment of novel protective gear

- Publications
  - 14th US National Congress on Comp Biomech, Montreal QC, July 2017
  - 43rd Northeast Bioengineering Conference, Newark NJ, April 2017
  - Annual Meeting of Biomed Eng Society, Minneapolis MN, Oct 2016

Fig 6. Torso prototype

21

Design of Experiments Approach to Optimizing Complex Bond Order and Reactive Potentials

Efraín Hernández-Rivera[1], S. Chowdhury[2], M.A. Tschopp[1] and S.P. Coleman[1]

[1]US Army Research Laboratory, **RDRL-WMM-F**, APG, MD, [2]University at Buffalo, Buffalo, NY
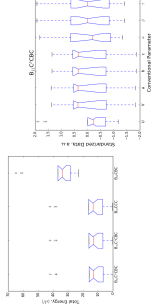
Research Objective

- Boron carbide's (B_4C) is ideal armor due to its lightweight and toughness
- Understand how it behaves atomistically
- State-of-the-art interatomic potentials under perform

Challenges

- B_4C is very complex: structurally, thermodynamically, i.a.
  - Requiring a robust potential
- Interatomic potential of interest, ReaxFF, tries to capture many physical processes

$$U = U_{bond} + U_{over} + U_{under} + U_{val} + U_{pen} + U_{tors}$$
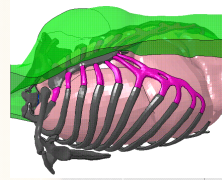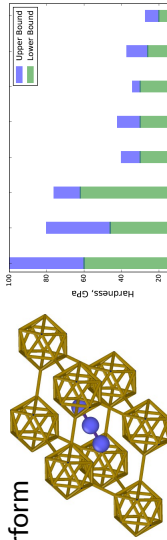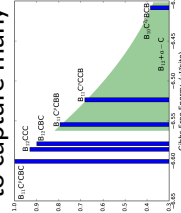$$+ U_{conj} + U_{vdWaals} + U_{Coulomb}$$
$$= \mathcal{F}[f(r_{ij}), g(r_{ij}, \theta_{ijk}), h(r_{ij}; q_i; q_j), \cdots]$$

Technical Approach

- Develop a systematic approach/framework for optimizing complex interatomic potentials

OFAT SA / Domain Red.   DoE (e.g. LHS)   Surrogate Selection & Training   Surrogate Re-training

$$\operatorname{OPT}_{X \in \mathbb{R}^n}[\mathcal{F}(X)]$$

SA: DGSM
$$\nu_{j,m} = \frac{1}{N}\sum_{i=1}^{N}\left(\frac{\partial F_m(\mathbf{x})}{\partial x_j}\right)^2 x_j$$
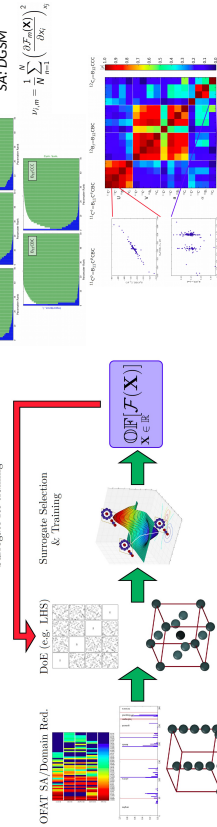
Accomplishments / Future Direction

Framework enables surrogate model based potential optimization

NSGA-II / Pareto Opt.

$U_m = 340 \pm 17/z$, $V_m = 29$ L/
$U_m = 110 \pm 0/z$, $V_m = 180$ L/

Expected Polymorph Order

B_{12}CBC	B_{12}CBC	B_{12}CBC
B_{12}CCC	B_{12}CCC	B_{12}CCC
B_{11}C'CBC	B_{11}C'CBC	B_{11}C'CBC
B_{11}C'CBC	B_{11}C'CBC	B_{11}C'CBC
DFT	GAND_x	ReaxFF

Initial surrogates included simple linear and combination effects, started exploring more complex surrogates (e.g. SVM)

Information from Failed Samples

B_{12}CCC B_{11}C'CBC

2D Surrogate Example

Atom 33

Hardness, GPa — dia-C, CBN, BCN, B_4O, B_4C, β-B, SiC, Al_2O_3 (Upper Bound / Lower Bound)

Relative Abundance — Gibbs Free Energy, (eV/atom) — B_{12}C'CBC, B_{12}CCC, B_{11}CBC, B_{12}C'CBB, B_{11}C'CBB, $B_{11}+v - C$, B_{12}CBC'CB

U.S. ARMY
RDECOM

Effect of a mid-build halt on the microstructure and porosity in powder bed fusion stainless steel parts

Clara Hofmeister, Andelle Kudzal, Joshua Taggart-Scarff, Ryan Rogers, Jennifer Sietins, & Brandon McWilliams

Weapons and Materials Research Directorate, Materials Division, Materials Manufacturing Technology Branch

Abstract

Interruption of builds during powder bed fusion (PBF) can occur if part or power failure occurs. An interruption of the build cycle may create a highly porous plane visible from the outside surface of the part known as a witness line. The effect of witness line on the microstructure of the part is unknown. In this study, the PBF of 17-4 stainless steel powder was intentionally halted mid-build for hold times ranging from 5 min to 12 hours and then allowed to continue. Microscopy and x-ray microcomputed tomography were conducted to determine the effect of hold time on the microstructure of the newly created heat affected zone as well as the size and morphology of the porosity in each witness line. The formation of witness lines and its effect on the quality of manufactured parts will be discussed.

Technical Approach

Experimental Design

Hold Time:
- 5 min   • 1 hr
- 10 min   • 3 hr
- 30 min   • 12 hr

- In this study we have purposefully stopped the build at specific locations to investigate the microstructure of the witness lines
- Parts were re-started under 2 conditions:
  1. No re-melting of previous layer
  2. Re-melting of previous layer

Experimental Setup

PROX DMP 100

$$E = \frac{P}{v \cdot h \cdot t} = 167 \frac{J}{mm^3}$$

Analytical Technique

- Metallographic Preparation
  - Polish to 0.02 μm with colloidal silica finish
  - Electrolytic etch
    - 10 g Oxalic Acid per 100 mL Water
    - 6 V DC, 60 sec
- Microscopy
  - Olympus DSX510 OM
  - Keyence VK-X200 Confocal Microscope

Zeiss Xradia 520 Versa μCT

Metals additive @ ARL

ARMY BENEFIT

Reduce logistics tail
- Mission readiness → "good enough" parts
- Optimize Structural Components → Light Weighing
- Reduce Number of Parts in Complex System → Reduce Cost
- Integrated Design of Materials and Manufacturing → Unique and Local Control of Microstructures and Properties

ProX 100: 4x4x4" Build Volume
ProX 300: 10x10x10" Build Volume
Full Volumetric Control of Build Parameters

Typical Microstructure

- 10% Oxalic Acid etchant dissolves carbides, strongly attacks sigma, moderately attacks austenite, does not attack ferrite*
- Bulk microstructure consists of a mixture of austenite and ferrite

*Vander Voort, G.F., Metallography Principles and Practice, 1984, McGraw-Hill, Inc. New York, p. 610-711.

Research Objective

What are Witness Lines?

…Also known as "witness marks"
- Typically caused by stoppage of the machine due to power, computer or part failure
- Visible on the outside surface of an as-built part
- May consist of a plane of pores
- Microstructure is unknown
- The effect on the mechanical properties is unknown

Porosity

Kudzal et al. unpublished work

Results/Discussion

Precursor Powder

Micrograph courtesy of Mr. Frank Kellogg
- Gas-atomized in N₂
- Average particle size: 14.5 μm
- Two phases: austenite and ferrite

62.9% Austenite
37.1% Ferrite

17-4 Alloy Composition*

*Radtke, S.B. and Auger, G. Wrought Stainless Steels. Properties and Selection: Irons, Steels, and High-Performance Alloys, Vol I, ASM Handbook, ASM International, 1990, p 841-907.

Porosity

No Re-melting

Re-melting

- No obvious plane of porosity was observed at each mid-build halt location regardless of halt time under these processing conditions

Types of Pores

Incomplete powder melting   Entrapped gas   Delamination

Summary

- Bulk microstructure consisted of ferrite and austenite
- Significant part growth (over spec) was observed
- A mid-build halt does not necessarily result in a plane of pores at that point in the build
- 3 types of pores were observed in the part:
  - Incomplete powder melting
  - Entrapped gas
  - Delamination porosity
- Witness line thickness ≈ 69 μm

Part Deviation

- Part tolerances were excellent around the diameter of the part
- A positive linear deviation was observed along the build direction of the part
- This quantified part deviation was used to correct for part growth during the build for all following analysis

Witness Line Microstructure

- Witness lines appear dark in contrast with the bulk microstructure
- Darkening of regions during etching can occur due to enhanced etching from localized grain refinement or due to the presence of an additional phase such as the sigma phase

Witness Line Thickness

No re-melting
Line Thickness ≈ 66 ± 16 μm

Re-melting
Line Thickness ≈ 73 ± 10 μm

- Witness lines are of similar thickness regardless of hold time
- The witness lines curve more in the sample with re-melting
- Both samples had roughly the same witness line thickness and therefore similar heat affected zones

Acknowledgments

U.S. ARMY RDECOM — Dr. Nicholas Ku (RDRL-WMM-E) — **ARL**

Synthesis and processing of nanocomposite ceramics for improved functionality of transparent materials

Dr. Victoria L. Blair (mentor, RDRL-WMM-E), Dr. Zackery Fleischman (PI, RDRL-SEE-L)

$Er:Y_2O_3 + MgO$

$ZnS + CaF_2$

Research Objective

- Need for laser host that combines high thermal conductivity and low max phonon energy, and also readily accepts the necessary rare earth dopants

Thermal gradient

Pump → Gain Medium → Laser emission

Waste heat

Ceramic nanocomposites
- Dual phase ceramics
- Mixture of materials
- Proper combination can benefit both phases

- Need for material system which combines high IR transmission with high strength for use in protective IR domes

➢ Multi-mode windows/domes
➢ Require small grain size for high strength and transmission

Technical Approach

- A majority high thermal conductivity phase (gray) and a minority low maximum phonon energy phase (red) with rare earth laser ions (green)

MgO
Er:Y$_2$O$_3$

- In-situ co-precipitation for nanoscale, intimately mixed powder

- Grain pinning reduces grain growth
  – Increased strength
  – Increased transmission range

- Hetereocoagulation using zeta potential

Challenges / Accomplishments

- Homogeneous mixing of powders is critical
- Rapid sintering is required to restrict excessive grain growth

Calcine Temp (°C)	Hot Press Dwell (min)
1000	10
700	10
700	30
1000	30

- Sintered samples reached ~95% of theoretical density
- Translucency achieved in sample
- Samples with best transmission exhibited most deficient fluorescence results in terms of intensity and structure

70 wt.% ZnS 30 wt.% CaF$_2$

80 wt.% ZnS 20 wt.% CaF$_2$

90 wt.% ZnS 10 wt.% CaF$_2$

	Zinc Sulfide	Calcium Fluoride
Density (g/mL)	sphalerite (cubic) = 4.10 wurtzite (hexagonal) = 3.98	3.18
Refractive Index	2.37	1.43
C.T.E. (10^{-6} °C^{-1})	6.8	18.9

ZnS experiences a phase transformation around the sintering temperature

CaF$_2$
ZnS
90 wt.% ZnS - 10 wt.% CaF$_2$
80 wt.% ZnS - 20 wt.% CaF$_2$
70 wt.% ZnS - 30 wt.% CaF$_2$

Wurtzite phase formation in ZnS suppressed with CaF$_2$ addition

Sample	Density (% TD)	Hardness (GPa)
100% ZnS	98.3	0.296 ± 0.005
90/10	97.7	0.270 ± 0.005
80/20	98.8	0.215 ± 0.004
70/30	98.6	0.191 ± 0.005

Planned Efforts in FY18

This work will continue in FY18, with Materials funding and leveraging of in-kind research from Photonics.

The purpose of this research effort is to advance synthesis and processing science for IR-transparent, dual-phase ceramic nanocomposites for expanded functionality and versatility in Army applications (sensor windows, domes, and mid-IR solid-state lasers). Other efforts will be made to:

- Optimize the composition to maximize lasing behavior while maintaining targeted microstructures (increase the overall Er content).
- Use fast sintering methods to maximize densification rate without encouraging grain growth.
- Continue spectroscopic characterization and modeling of scattering losses.

- Synthesize nanopowders and complete heterocoagulation to produce homogenous powders.
- Optimize composition to minimize grain coalescence and maximize grain pinning to maintain small grain size.
- Measure hardness and transmission of dense, nanoscale-grained parts.

Multiscale Coarse-Graining with Effective Polarizabilities: A fully bottom-up Approach

Patrick G. Lafond, Sergei Izvekov

WMRD, Lethality Division, Energetic Materials Science Branch

Coarse-Grain Models

Coarse-grain (CG) models offer a way to estimate large scale systems through reduced site representation. For example, the center of mass (CoM) of a molecule:

Fewer sites
↓
Fewer interaction
↓
Faster simulation!
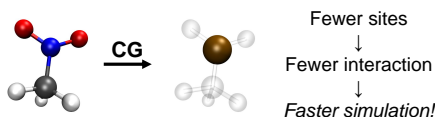
Fig 1. CG representation of nitromethane

When using CG models we lose fine detail information. For example: electrostatic interactions. *Real* molecules will respond to electric fields, but CG models won't
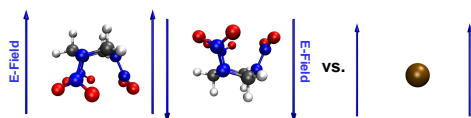
Fig 2. RDX conformational changes induced by e-field

Many properties, such as energetic sensitivity depend on electronic interactions. We want to develop a method to recover at least the charge and dipoles of CG models.

New Method

The CoM and diople of an n-atom molecule are defined by 6 variables: $(X_{CoM}, Y_{CoM}, Z_{CoM})$ and (μ_x, μ_y, μ_z) computed by:

$$(1) \quad \begin{bmatrix} m_1 & m_2 & \cdots \\ q_1 & q_2 & \cdots \end{bmatrix} \begin{bmatrix} r_1 \\ r_2 \\ \vdots \end{bmatrix} = \begin{bmatrix} M_{Tot} R_{CoM} \\ \mu \end{bmatrix} \quad \text{or} \quad \mathbf{w}\vec{r} = \{R_{CoM}, \mu\}$$

In the special case of $n = 2$ sites ("+" and "-"), there are only 6 degrees of freedom: (X_+, Y_+, Z_+) and (X_-, Y_-, Z_-)

$$(2) \quad \begin{bmatrix} M_+ & M_- \\ Q_+ & Q_- \end{bmatrix} \begin{bmatrix} R_+ \\ R_- \end{bmatrix} = \begin{bmatrix} M_{Tot} R_{CoM} \\ \mu \end{bmatrix} \quad \text{or} \quad \mathbf{W}\vec{R} = \{R_{CoM}, \mu\}$$

So there is a *unique* mapping of CoM + dipole to a 2-site dimer meaning $\mathbf{W}^{-1}$ exists
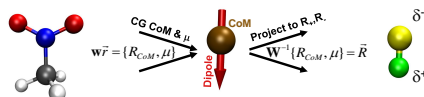
Fig 3. How coordinates are projected to dimer representation

This lets us convert molecules into dimers that match the instantaneous CoM, charge, and dipole. The trajectory of dimers defines a training set to build CG force fields.

Results for Liquid Systems

We first tested with nitromethane to see how the method performs with small liquids
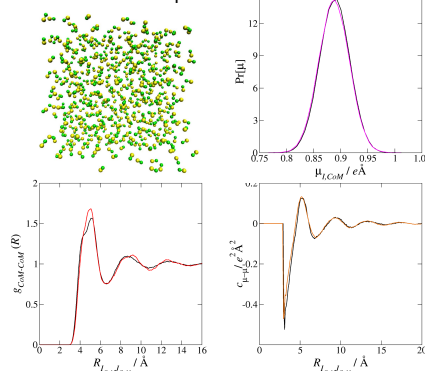
Fig 4. Picture of CG simulation (top left)Comparison of CG (color) to atomistic (black) properties. Dipole distribution (top right), RDF (bottom left) and dipole-dipole correlation. (bottom right)

Extended method to derive intra-molecular potentials with poly(vinyl alcohol)
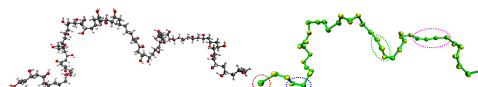
Fig 5. Comparison of atomistic PVA (left) and CG PVA (right)
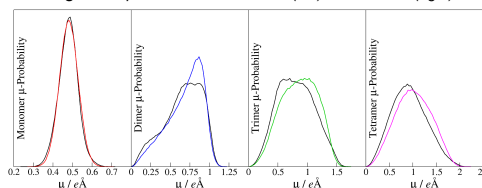
Fig 6. Comparison of intra-chain dipoles for atomistic (black) and CG PVA (colored). Sample segments highlighted in Fig 5.

Outlook

The method presented matches the centers of mass and first 2 terms of the multipole expansion allowing for bottom-up models that interact with external fields.

Preliminary results show the method also works for crystalline RDX meaning better prediction of energetic sensitivity in the near future.
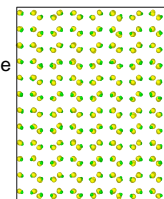
Fig 7. CG RDX matching native crystal structure

Femtosecond Laser Machining of Micro-tensile Specimens for High Throughput Mechanical Testing

Daniel J. Magagnosc[1], Jonathan P Ligda[2], Tomoko Sano[2], Brian E Schuster[1]
[1]WMRD, Lethality, Lethal Mechanisms, [2]WMRD, Materials, Lightweight and Specialty Metals

Research Objectives

Goal: Use micromechanical tests to isolate deformation mechanisms

- Material deformation accommodated by a diversity of mechanisms
  1) Dislocation Interactions 4) Grain Boundary Sliding
  2) Deformation Twinning 5) Intergranular Fracture
  3) Secondary Phases 6) Intragranular Fracture
- Isolating and characterizing individual mechanisms critical to constitutive model development
- Property-performance relationships key to future materials development and application

Challenge: Established small-scale testing methods restricted by sample geometry or throughput

Indentation	Uniaxial Loading	Cantilever Bending

G. Pharr and W. Oliver, *MRS Bulletin*, **17** (1992). M. D. Uchic and D. M. Dimiduk, *Mater. Sci. Eng. A*, 400-401 (2005). J. P. Best et al., *Scripta Materialia*, 112 (2016).
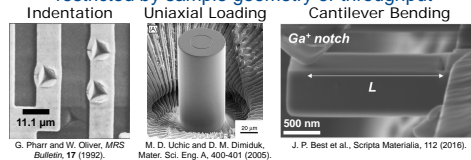
New high throughput fabrication and testing methods are required

Experimental Results

FS-laser machining produces high quality tensile specimens

- Gage widths less than 100 µm easily fabricated
- Laser machined samples show sharp, clean edges
- Sub-micron surface structuring, characteristic of FS-laser machined surfaces, observed
- Resulting samples show signs of minimal damage and are ideal for mechanical testing
- Tensile tests conducted with *in situ* imaging

Laser micromachining compatible with wide range of materials

As-Rolled Aluminum	Sintered Silicon Carbide	Impact Modified PMMA
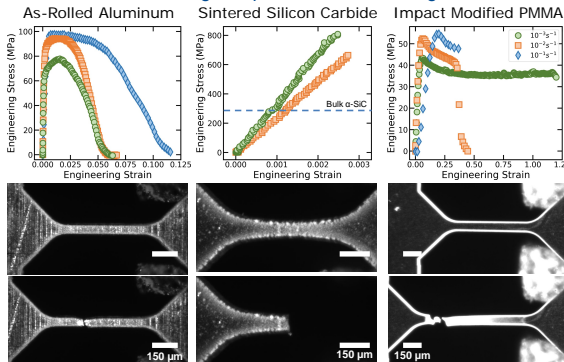
FS-laser machining does not influence measured microtensile material response

Technical Approach

Femtosecond laser based sample fabrication avoids limitations of established small-scale methods

- Femtosecond (10^{-15} s) laser pulses produce high energy density and overcome ablation threshold
- Ultrashort interaction minimizes damage in material

K.-H. Leitz, et al., Phys. Procedia, **12** (2011).
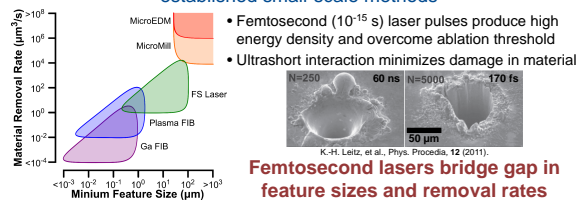
Femtosecond lasers bridge gap in feature sizes and removal rates

New laser machining methods enables high throughput fabrication

Rough Outline	Serial Contours	Final Cleaning
V=0.2 mm/s, N=3	V=0.6 mm/s, N=1, 25 contours, 2 µm spacing	V=0.6 mm/s, N=50
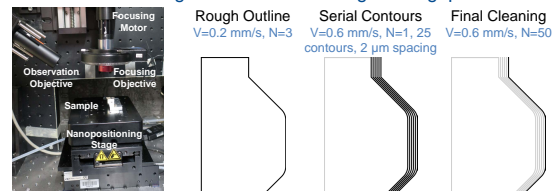
Challenges and Future Directions

Challenges limiting broad application of FS-laser machining

- Methods restricted fabrication from thin (50 µm or less) sections
  For materials greater than 50 µm, machining time rapidly increases
  Characterize most efficient machining feed rates and path spacing
  Further optimize machining process for time efficiency
- Reliable method for preparing large area thin sections needed
  Commercial sources for many materials are available
  Wedge polishing facilitates producing thin sections over large areas
- Minimum achievable feature size
  Feature size related to focused spot size and ablation threshold
  Additional focusing objectives and apertures required

Future applications and opportunities

- Microscale fracture toughness investigations
  Observed fracture toughness highly geometry dependent
  High material removal rates enables large ligaments in miniaturized fracture tests
  Example: Fused quartz, intermetallic precipitates, transparent armor ceramics
- Targeting microstructural features
  Identify features with optical or electron microscopy, electron back scatter diffraction
  Machine tensile bar to include feature of interest and use in situ loading to monitor behavior
  Example: deformation twinning in magnesium
- High throughput testing for statistical analysis
  Stochastic deformation processes require statistically significant sample sizes
  Small sample volumes and short fabrication times ideal for large sample sizes
  Example: Tensile behavior in armor ceramics (silicon carbide, boron carbide, alumina)

Evaluation of Microporous and Micro-Mesoporous Solid Acid Zeolites for Ethene to Hydrocarbons

U.S. ARMY RDECOM

ARL

Drs. Luther Mahoney (presenter),
Laleh Emdadi, Zachary Dunbar
Co-Advisor: Dr. Dat T. Tran
Advisor: Dr. Ivan C. Lee, (301) 394-0292

Abstract

The study evaluated microporous and micro-mesoporous solid acid catalysts for converting ethene to liquid hydrocarbons. Our hypothesis is that using novel solid acid catalyst we can increase the energy dense liquid hydrocarbon yield with a reduction in coke fouling of the catalyst. Further, we hypothesize that optimized metal dopant loading will increase the liquid hydrocarbon yield from introduction of Lewis acid sites. The results show that using two-dimensional zeolites as solid acid catalysts can produce the largest liquid hydrocarbon yield. A comparison of three-dimensional zeolites showed lower liquid product yield. Likewise, the metal-loaded zeolites in two-dimensions and three-dimensions using gallium and zinc at two-percent produced more hydrocarbon liquid. The yield of liquid hydrocarbons was up to 38% zinc loaded Pillared-MFI. The conversion to of ethene to products ranged from 97 to 99%. These results will be used in converting 20% aqueous ethanol to liquid hydrocarbons.

Background

Porous materials can be classified according to pore diameter: (1) microporous (< 2 nm); (2) mesoporous (2-50 nm); and (3) macroporous (> 50 nm). Typically, the smaller the pore diameter leads to pore blockage and reduced mass-transfer. Lower mass-transfer enables greater chance to form undesired products. Solid acid catalysts are used largely in developing or converting smaller compounds to larger more dense structures. The most used solid acid catalysts are microporous zeolites.

Key variables of zeolites:
1. Si/Al ratio
2. Bronston acid strength
3. Lewis acid strength, dispersion, and loading
4. Textural properties: Pore diameter, pore volume, and surface area.
5. Dopant type and metal loading
6. Reaction variables: Space velocity, pressure, and temperature
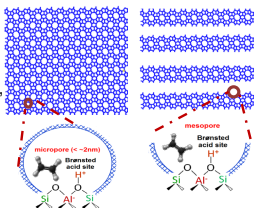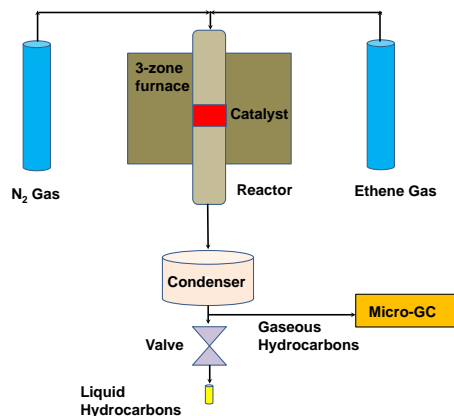
Left: Micropore; Right: Mesopore

Laleh Emdadi, Ph.D.

Experiment

Results

- Among the nine base and metal-doped zeolites, the 2%-Zn-Pillared-MFI catalyst gave the largest liquid product yield.
- The WHSV appeared to have an impact on the liquid product yield. Lower WHSV gave the largest liquid product yield.
- The contact time was observed to have a large influence on liquid product yield. Low contact times gave only gas-phase hydrocarbons. Large contact times gave large liquid product yield..
- Thermal-Gravimetric-Analysis (TGA) suggested that the pore geometry influenced the coke amounts and coke species

Gas-Phase micro-GC analysis time-on-stream

Liquid product after eight-hour conversion
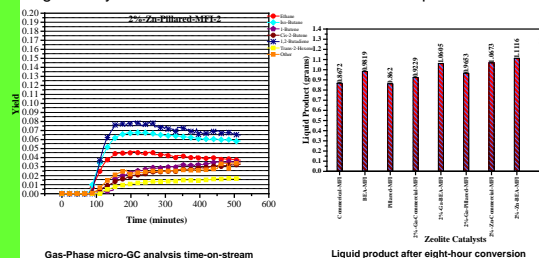
Theoretical Yield: Ethene to Benzene	
Catalyst	Yield (%)
Commercial-MFI	28.7
BEA-MFI	32.5
Pillared-MFI	28.5
2%-Ga-Commercial-MFI	30.5
2%-Ga-BEA-MFI	35.1
2%-Ga-Pillared-MFI	31.9
2%-Zn-Commercial-MFI	35.3
2%-Zn-BEA-MFI	36.8
2%-Zn-Pillared-MFI	38.3
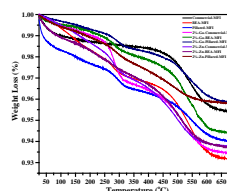
The BEA-MFI has the largest weight loss. The 2%-Zn-Pillared-MFI and Pillared-MFI has the smallest weight loss.

Discussion/Path Forward

Scientific Questions:

Does the pore geometry play a major role in the liquid product yield, gas-phase yield, and coke fouling? Additionally, what is the influence of the metal dopant on the zeolite material? Is the reaction conditions, catalyst loading, and dopant levels amendable to study of aqueous ethanol to hydrocarbons reaction?

Next Steps:

1. Complete two reactor system using the reaction conditions, catalyst loading, and dopant levels to determine the liquid product yield and product distribution.
2. Complete TGA analysis of used catalysts in two reactor system to see if the products amounts are similar to only use of ethene.
3. Complete DRS-UV-Vis analysis of two-reactor system used catalyst to learn what organic coke species are present.

U.S. ARMY RDECOM

EXTRACTION OF METAMATERIAL CONSTITUTIVE PARAMETERS USING THE FIRST-PRINCIPLE HOMOGENIZATION THEORY

ARL

Quang Nguyen and Amir I. Zaghloul
US Army Research Laboratory, SEDD, Adelphi, MD, 20783
93nguyen@cua.edu, **amir.i.zaghloul.civ@mail.mil**

Objectives

- Accurate and reliable techniques for the constitutive parameters extraction are essential to characterize and design metamaterials
- Implement the first-principle homogenization theory (FPHT) to determine the effective permittivity, ε, and permeability, μ, for an infinite 3D array consisting of split-ring resonator (SRR) inclusion

Current Homogenization Techniques

- Nicolson-Ross-Weir (NRW) methods are formulated by inverting Fresnel equations

$$S_{11} = \frac{R_{01}\left(1 - e^{i2nk_0 d}\right)}{1 - R_{01}^2 e^{i2nk_0 d}}$$

$$S_{21} = \frac{\left(1 - R_{01}^2\right)e^{ink_0 d}}{1 - R_{01}^2 e^{i2nk_0 d}}$$

$$R_{01} = \frac{z-1}{z+1}$$

$$e^{ink_0 d} = \frac{S_{21}}{1 - S_{11}\dfrac{z-1}{z+1}}$$

$$n = \frac{1}{k_0 d}\left[\begin{array}{c}\left\{Im\left[ln\left(e^{ink_0 d}\right)\right] + 2m\pi\right\} \\ -i\,Re\left[ln\left(e^{ink_0 d}\right)\right]\end{array}\right]$$

$$z = \pm\sqrt{\frac{\left(1+S_{11}\right)^2 - S_{21}^2}{\left(1-S_{11}\right)^2 - S_{21}^2}}$$

$$\varepsilon = \frac{n}{z}$$

$$\mu = nz$$

- Violation of the passivity condition on resonant bands (wrong sign of ε'' and μ'')
- Appearance of non-physical elements such as anti-resonance for ε' and μ'
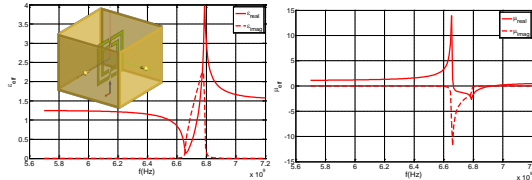
First-Principles Approach

- Base on the original Claussius – Mossotti formulas
- Utilize the polarizabilities of a single resonant inclusion to extract the bulk effective parameter of a 3D periodic array of inclusion
- The final expression of bulk the effective parameters using FPHT is written in a generalized Claussius – Mossotti closed form as

$$\varepsilon_{eff} = \varepsilon_0\left[1 + \frac{1}{d^3}\frac{\alpha_m' - C_{int}}{\left(\alpha_e' - C_{int}\right)\left(\alpha_m' - C_{int}\right) - C_{em}'^2 + \alpha_{em}'^2}\right],$$

$$\mu_{eff} = \mu_0\left[1 + \frac{1}{d^3}\frac{\alpha_e' - C_{int}}{\left(\alpha_e' - C_{int}\right)\left(\alpha_m' - C_{int}\right) - C_{em}'^2 + \alpha_{em}'^2}\right].$$

$$\alpha_m' = \frac{\alpha_e}{\alpha_e\alpha_m + \alpha_{em}^2}$$

$$\alpha_e' = \frac{\alpha_m}{\alpha_e\alpha_m + \alpha_{em}^2}$$

$$\chi_{xy,eff}^e = \frac{1}{d^3}\frac{c_0^{-1}\alpha_{em}'}{\left(\alpha_e' - C_{int}\right)\left(\alpha_m' - C_{int}\right) - C_{em}'^2 + \alpha_{em}'^2}$$

$$\chi_{xy,eff}^0 = \frac{1}{d^3}\frac{c_0^{-1}C_{em}'}{\left(\alpha_e' - C_{int}\right)\left(\alpha_m' - C_{int}\right) - C_{em}'^2 + \alpha_{em}'^2}$$

$$C_{int} = C - \left[\frac{1}{d^3}\frac{k_0^2}{\beta^2 - k_0^2}\right]$$

$$C_{em}' = C_{em} - \left[\frac{1}{d^3}\frac{\beta k_0}{\beta^2 - k_0^2}\right]$$

where α_e, α_m and α_{em} are the electric, magnetic, and magnetoelectric polarizability coefficients, respectively. C and C_{em} are the interaction constant. β is the complex wavenumber. χ^e and χ^o are associated with magnetoelectric coupling effects at the inclusion and lattice level, respectively. "*Effective*" is defined as macroscopic averaged quantities of periodic collections of inclusions

Simulations Results
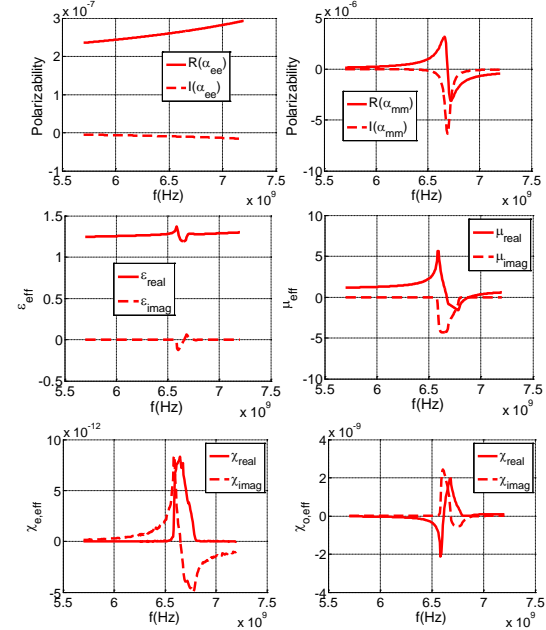
References

- A. M. Nicolson, G. F. Ross, "Measurement of the intrinsic properties of materials by time domain techniques." *IEEE Trans. Instrum. Meas.*, vol. IM-17, pp. 395-402, Dec. 1968.
- W. B. Weir, "Automatic measurement of complex dielectric constant and permeability at microwave frequencies.", *Proc. IEEE.*, vol. 62, pp. 33-36, Jan. 1974.
- A. Alu. "First-principles homogenization theory for periodic metamaterials." *Physical Review B*, vol. 84, no. 7, 2011.

28

Development of a Hybrid Vehicle Capable of Performing Aggressive Maneuvers with On-board Sensing

Steve Nogar

VTD - Autonomous Systems Division - Microsystems and Mechanics Team

stephen.m.nogar.ctr@mail.mil

Research Objective

• Small, autonomous micro air vehicles (MAVs) are an important technology that enables improved surveillance and reconnaissance compared to larger vehicles, especially in urban and indoor environments. As the vehicle size decreases (<30 cm), they become increasingly constrained to specialized flight conditions, mission profiles, environments, and sensor packages.

• Develop a MAST scale vehicle with increased versatility that is capable of hover, efficient forward flight, and can perform a controlled transition between the two states.

• Relevant control algorithms for maintaining stability through transition for the underactuated vehicle.

• Develop on-board sensing capabilities that can enable aggressive maneuvers including perching with a focus on monocular vision techniques that take advantage of improved on-board computing capabilities.

Approach

• Develop hybrid vehicle capable of vertical take off and landing (VTOL) using a dual articulated rotor design

• Use off the shelf components like the Snapdragon Flight to enhance onboard processing capabilities

• Develop relevant control and dynamics models to enable controlled transition

• Demonstrate transition using motion capture

• Develop aggressive flight capabilities and demonstrate perching maneuver using motion capture

• Achieve autonomous landing in a GPS denied environment using a marked target

• Achieve perching using only on-board sensing

Qualcomm Snapdragon Flight Kit
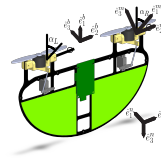
Status and Accomplishments:

• Developed a cascaded, nonlinear backstepping controller that can transition between forward flight and hover

• Verified controller performance numerically

• Designed and constructed vehicle

• Implemented control algorithms on-board using robot operating system (ROS) and PX4 flight controller

• Demonstrated controlled transition using motion capture system

• Confirmed improved efficiency in forward flight mode

• Characterized vehicle force and moment capabilities

• Verified adverse pitching moments do not inhibit control

Future Direction

• Modify vehicle to fly outdoors and use GPS for position estimation

• Collaborate with University of Pennsylvania to perform aggressive maneuvers with aid of motion capture system

• Implement visual odometry using monocular camera to aid in state estimation

• Implement monocular vision algorithms to obtain vehicle pose relative to a known target landing site with a focus on fast and efficient vision methods

• Perform autonomous landing and perching without external state feedback

Comparison of pitching moments generated by tilting rotors
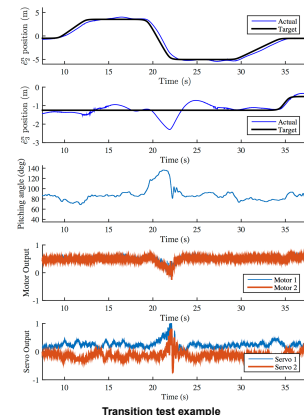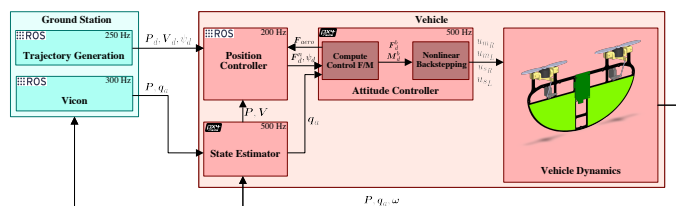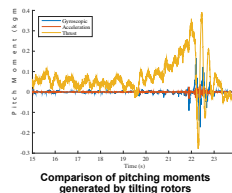
Transition test example

U.S. ARMY RDECOM® — ELECTROLYTES FOR NEXT GENERATION LITHIUM BATTERIES — ARL

Materials Research>Energy and Power>Energy Storage
Tactical Unit Energy Independence
POC: Dr. Marshall Schroeder, marshall.a.schroeder.ctr@mail.mil

Funding Type: 6.1, Mission
Project Size: Small
Duration: Start 2016 – Expected End 2020

OBJECTIVES

Commercial Li-Ion → Stable Electrolyte → 5V Class Li-ion

Operation: OEF (2014)
72 Hour Mission
16lbs Batteries/Soldier Kit
672lbs/Platoon
9W Average Energy/Soldier
SOA Li-Ion (90 Wh/kg)

Future Readiness
120 Hour Mission
8lbs Batteries/Soldier Kit
336lbs/Platoon
15W Average/Soldier
Future Li-Ion (500 Wh/kg)

UNBURDEN THE WARFIGHTER
- Formulate electrolytes for next generation lithium battery chemistries that are lightweight with improved performance metrics to reduce the weight of deployed energy sources
- Develop safer, non-flammable electrolyte chemistries which remain stable even under normally catastrophic battery conditions (cell puncture, shorting)

NEW DEGREES OF FREEDOM IN TACTICAL ENERGY
- Expand temperature window of operation of electrolytes to accommodate battery operation in aggressive new mission environments
- Unlock new electrode/electrolyte chemistries with unprecedented power/energy densities for extended mission durations and high-power weapons/sensors
- Enhance stability of electrolytes for long operational life and flexibility in hybrid energy storage systems

CHALLENGES
SCIENTIFIC/ARMY

Molecular orbital theory illustrates how SOA electrolytes do not translate well to next generation battery systems.
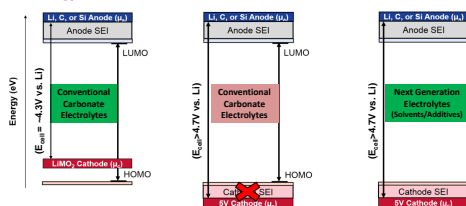
- Electrolyte stability can be compromised by each battery element (anode/cathode/separator/current collectors/cell packaging) depending on temperature and cycling conditions, particularly in HV systems.

APPROACH
- New solvents with superior intrinsic anodic stability (nitriles, sulfones, fluorinated solvents)
- Experiment with different salt chemistries and concentrations, as pioneered by Yamada et al., Lucht et al., Aurbach et al., and others in the field
- Additives for interphase stabilization: molecular engineering with empirical studies backed by molecular dynamics calculations.
- Half/Full Cell Testing

RESULTS

LNMO/MCMB full cell cycling data @30°C (top left) and 55°C (top right) showing substantial improvements in the ARL system over the commercial.
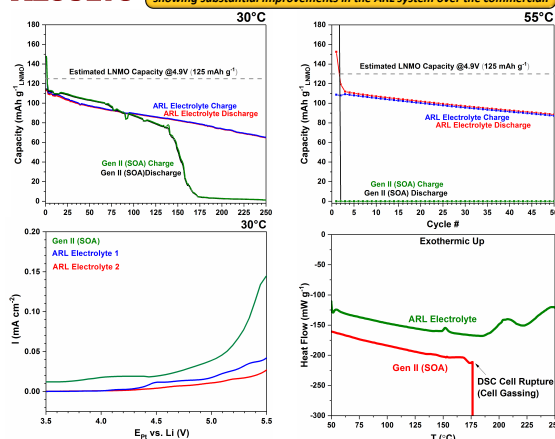
Anodic linear sweep voltammetry of Pt in different electrolytes illustrating HV stability of ARL electrolyte (left). Differential scanning calorimetry (DSC) of ARL and commercial electrolyte showing high temperature stability.

- Electrolytes developed at ARL achieve remarkable levels of capacity retention and stability in an aggressive high voltage system (4.9V), eclipsing the commercial SOA, especially at high temperature
- In addition to generating less gas (parasitic) than the commercial SOA, the recently developed ARL electrolyte is non-flammable, even under direct ignition from an acetylene welding torch
- Extremely rare demonstration of reversible graphite anode reaction in an EC-free electrolyte formulation

DISCUSSION & CONCLUSIONS
- Fundamental studies of solvation behavior as a function of solvent/salt/concentration garner insight into developing new high performance systems
- Temperature and voltage windows of operation can be expanded, unlocking promising new electrodes.
- The properties/stability of these formulations have an extensive range of potential applications beyond batteries. (Capacitors, hybrid storage systems, etc.)

PATH FORWARD
- Continued optimization, testing, and characterization will lead to further IP and potential scale-up efforts with Industry/Academic collaborators (SAFT/Batt500)
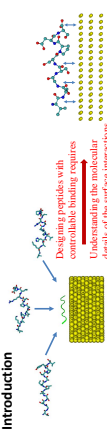
PUBLICATIONS & RECOGNITION
- Alvarado, J., Schroeder, M., Xu, K. et al. *Advanced Energy Materials.* **Submitted May 2017**
- ARL Invention Disclosure: ARL 17-25 (**May 2017**)
- Xu, K. *Chemical Reviews, 2014*

Approved for public release; distribution is unlimited.

DFT Calculations of Arg and Lys on Au(111) to Probe the Effects of Amino Acid Conformation and Dispersion on Binding

Meagan C. Small, Jessica L. Terrell, Deborah A. Sarkes, Justin Jahnke, Dimitra N. Stratis-Cullum, and Margaret M. Hurley

Abstract

Biomolecular-inorganic hybrid materials have many potential applications in medicine, electronics, and nanotechnology. Of great interest is designing peptides that have predictable and controllable binding to inorganic surfaces, which requires a detailed understanding of the binding interactions between the amino acids and inorganic surface. Computational models have provided key insight into the underlying intermolecular interactions in such systems, including probing the effects of dispersion and hydration. However, owing to limited computational resources, these studies are often performed using periodic models where care must be taken to understand the effects of model size and periodicity, as well as any possible additional limitations in the method. In this study, we have performed quantum mechanical (QM) calculations at the DFT level of theory for the side chains of Arg and Lys on an Au(111) slab that is of sufficient size to mitigate periodicity-based artifacts. Furthermore, multiple orientations of the amino acid on the slab have been calculated with and without dispersion to compare the effects of conformation and dispersion on binding. The results show that most favorable orientations differ significantly when dispersion is explicitly included. For Arg, the guanidinium group is oriented perpendicularly to the surface when dispersion is not included and planar when dispersion is added. Similarly, the alkyl chain of Lys lays flat along the surface of the slab when dispersion is included, yet tends to be at a diagonal with the amine closest to the surface in the absence of dispersion. Lastly, the results will be discussed in the context of existing computational and experimental data for the binding of amino acids on Au(111), as well as the potential for using this data to refine existing bio-inorganic force fields (FFs) and guide future model development of peptides on inorganic surfaces.

Introduction

Designing peptides with controllable binding requires

Understanding the molecular details of the surface interactions

- Mixed biomolecular-inorganic systems are of interest for a diverse set of applications, including sensors, electronics, medical devices.
- It is necessary to understand the molecular details of bioorganic-inorganic interactions in order to **rationally design peptides with controllable binding**.
- To date, QM models have provided great insight into organic-inorganic interactions.
  - Studies of amino acids on gold have investigated the relative binding affinities for different amino acids.
  - Combined QM (DFT) and MD studies have demonstrated that amino acid binding to gold surfaces is an interplay between steric and electrostatic factors (Hoefling 2010), including charge transfer (Hong 2009).
- Yet, these studies are limited by the inherent challenges in employing molecular models including:
  - QM models utilizing smaller gold slab models owing to limited computational resources.
  - The analysis of a single amino acid conformation
- Previously, DFT methods were used in combination with MD simulations using CHARMM-GolP FF to calculate the MOST FAVORABLE conformations of the amino acids on Au(111) (Hoefling et al. (2010))
  - Effects of solvation and the peptide backbone were important contributors to the preferred orientation of the amino acid side chain.
  - Minimum orientation for the ARG side chain (guanidinium) is different between the gas phase DFT calculations versus solvated MD simulations.
- This study is intended to **improve our understanding of how amino acid conformation affects binding** to an Au(111) surface
  - We use DFT methods to determine the relative energies for a number of ARG and LYS orientations on Au(111).
  - We also calculate the respective MM energies using INTERFACE (Heinz 2012).

References

1. Frisch, M. J.; et al.; Pople, J. A. *Guassian03*, Guassian, Inc.: Wallingford, CT, **2004.**
2. MacKerell, A. D.,Jr.; et al.; Karplus, M. *J Phys Chem B* **1998,** 102, 3586-3616.
3. MacKerell, A. D.,Jr.; Feig, M.; Brooks, C. L., 3rd. *J Comput Chem* **2004,** 25, 1400-15.
4. Brooks, B. R.; et al.; Karplus, M. *J Comput Chem* **2009,** 30, 1545-1614.
5. Heinz, H.; et al.; Emami, F. S. *Langmuir* **2012,** 29, 1754-1765.
6. Wright, L. B.; et al.; Walsh, T. R. *J Comput Theor Chem* **2013,** 9, 1616-1630
7. Hoefling, M.; et al.; Gottschalk, K.-E. *ChemPhysChem* **2010,** 11, 1763-1767
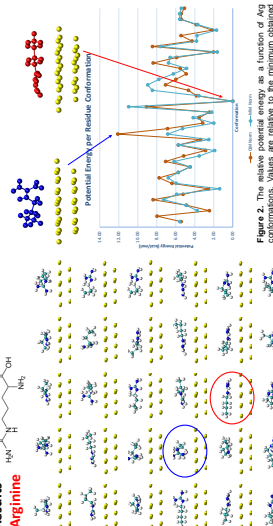8. Hong, G.; et al.; Pachter, R. *Applied Materials & Interfaces* **2009,** 1, 389-392

Results

Arginine

Figure 1. The conformations of Arg on Au(111) studied in this work.
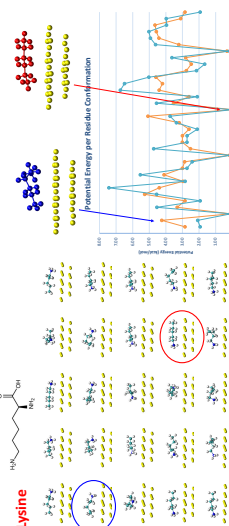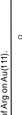
Dispersion   **No dispersion**

Figure 2. The relative potential energy as a function of Arg conformations. Values are relative to the minimum obtained from QM.

Figure 3. Comparison of the conformations obtained with and without dispersion. Distances shown are based on non-hydrogen atoms.

Figure 4. Top view of the lowest (left) and highest (right) energy conformation of Arg on Au(111).

Lysine

Figure 5. The conformations of Lys on Au(111) studied in this work.

Dispersion   **No dispersion**

Figure 6. The relative potential energy as a function of Lys conformations. Values are relative to the minimum obtained from QM.

Figure 7. Comparison of the minimum orientations obtained with and without dispersion. Distances shown are based on non-hydrogen atoms.

Figure 8. Top view of the lowest (left) and highest (right) energy conformations of Lys on Au(111).

Methods

All QM calculations were performed using Gaussian09 (Frisch 2004), employing the B3LYP/6-31G** level of theory for the amino acids and B3LYP/LANL2DZ level of theory for gold. Empirical dispersion was included using the GD3BJ method. Only amino acid side chains were studied, with the terminal COOH and NH$_2$ groups replaced by hydrogens. Gold atoms were fixed throughout the calculation. MM calculations were performed with CHARMM, version 41c2 (Brooks 2009), using the CHARMM36 protein (MacKerell 1998, MacKerell 2004a,b) force field for the amino acids and INTERFACE force field (Heinz 2012) for the gold non-bonded terms. QM-optimized coordinates were used for calculation of the MM energy profiles.

An Au(111) gold slab of dimensions 10.8 x 11.5 x 2.4 Å (for a total of 32 Au atoms) was constructed using the unit cell of Heinz (2012). Initial residue conformations on the gold were first generated in CH-ARMM in which the residue was translated to be 7 Å from the surface of the gold slab and subjected to 50 steps of minimization using steepest descent (SD). Gold atoms were fixed for all geometry optimizations. Additional residue orientations were constructed by rotating the amino acid in the x and y planes by increments of 15° up to 360°, with rotated orientations minimized using 500 steps of SD and 100 steps of conjugate-gradient.

In the QM calculations including dispersion, additional orientations were also considered. First, optimized conformations were aligned with respect to the non-hydrogen atoms of the amino acid and the RMSD was calculated using the VMD Trajectory Tool (REF). Unique conformations were selected in which the RMSD > 0.005 Angstrom. From each unique conformation, three additional orientations were generated by rotating the C2-NE-CD-CG, NE-CD-CD-CB, and CD-CG-CG-CA (ARG) and CA-CB-CG-CD, CB-CG-CD-CE, and CG-CD-CE-NZ torsions by 180°, which were then subjected to the same minimization as above.

Discussion

- To the best of our knowledge, this is the first study **to systematically investigate the effects of residue orientation on binding to Au(111).**
- Our non-dispersion QM minimum orientations are comparable to those found in previous studies using DFT/MD Hoefling et al. (2010).
- For the most part, classical and QM energy profiles over side chain orientation are similar at the current level of theory → for both ARG and LYS.
  - ARG: out of 40 conformations studied, 2 conformations are > 2 kcal/mol relative difference.
  - LYS: out of 34 conformations, 1 is > 2 kcal/mol relative difference.
- With respect to side chain orientation, at the current level of theory ARG and LYS have a wide distribution of conformations that affect the potential energy profile.
  - ARG varies by ~ 12 kcal/mol and LYS varies by ~ 5 kcal/mol
- ARG and LYS maintain heavy atom distances of ~ 3.3 Å from the Au(111) surfaces at the current QM level.
- The most favorable conformations for ARG and LYS orientations are relatively flat along the gold slab → maximize VDW contacts.
  - When dispersion is not included, the orientations are significantly different.

Future Directions

- Further investigations are underway to understand the **response of the gold** to the presence of the amino acids and how the residue conformation modulates that response
- Comparison of available biomolecular-inorganic FFs (e.g. INTERFACE and CHARMM-GolP (Wright 2013)) will be performed.
  - Because conformational properties are highly FF-dependent, it is important that the FF accurately describe the interactions between the amino acid and gold, including relative energy profiles for a number of side chain orientations on Au(111).
  - Hence, possible pairwise-specific LJ (NBFIX) terms may be required to recapture the relative energy profiles and effects of dispersion.

Conclusions

- We have presented DFT calculations of a number of ARG and LYS orientations on a slab of Au(111).
- For the ARG orientations, the maximum conformation was 12 kcal/mol higher than the minimum and corresponds to a conformation in which the guanidinium groups is oriented perpendicular to the slab, rather than planar, thereby limiting contact of the amines with the gold. For the LYS orientations, the minimum was 5 kcal/mol higher than the minimum and corresponds to a CD and CG methylene groups are slightly raised from the slab surface, thereby lowering the VDW interactions.
- The classical energies as calculated by INTERFACE (Heinz 2012) are largely within 2 kcal/mol of their respective DFT-based energies, though a few exceptions do occur that are the subject of ongoing analysis.

Acknowledgements

Acoustic Wireless Power Transfer

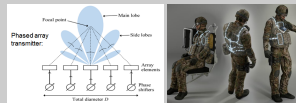## Victor F.-G. Tseng, Sarah S. Bedair, Nathan Lazarus
Sensors and Electron Devices Directorate, E&P Division, Power Components Branch

Introduction

Advantages of acoustic WPT:
- **Higher efficiency than inductive at larger distances** (acoustic focusing)
- Smaller transducers, lower frequencies
- Transmits through air, water, or metal

Army relevance:
- On-soldier powering of wearable & portable devices
- Wireless power on board munitions
- Structural health monitoring, embedded sensors

Through air Acoustic WPT

1) Phased array transmitter (acoustic focusing):
- Increases power transfer efficiency in near field region
- Enables adaptive focal point tuning (beam steering)

37 element transmitter array demo:
- Continuous wave, 40 kHz transmission

Adaptive focal distance tuning:
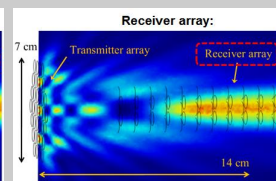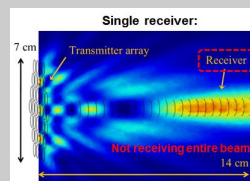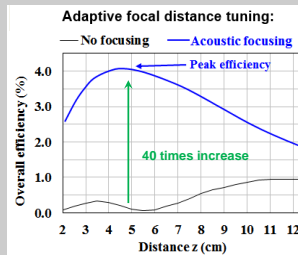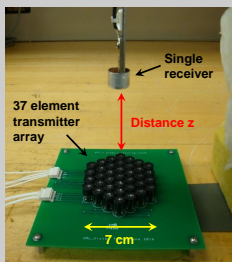
2) Receiver array for improved efficiency:
- Increases efficiency due to larger receiver area
- Larger improvements at larger distances
- Power combining between receiver array elements
  - Uniform input power needed to maximize efficiency
  - Series interconnection for lower load
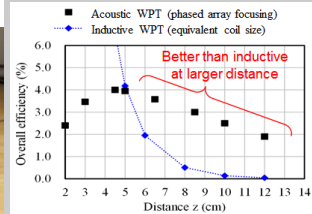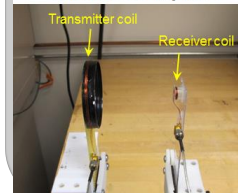 - Parallel interconnection for higher load

7 element receiver array demo:
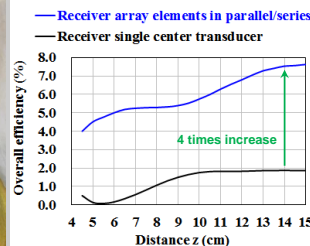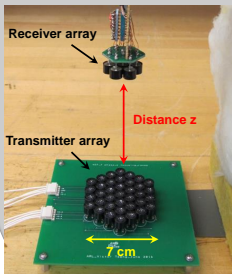
Acoustic WPT vs Inductive WPT

- Compared to Inductive WPT with coils of equivalent area
- Acoustic wins over Inductive at larger distances

Through metal power & data transfer

- Acoustic waves can propagate through metal
  - EM waves are blocked by metal
- Higher efficiencies can be achieved due to low reflections

Power & data transfer to embedded sensor:
- Combine acoustic receiver, sensor, electronics in system
- Transfer power to system embedded in metal
- System responds with sensor signal
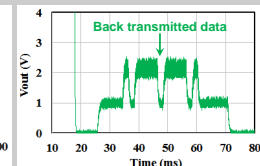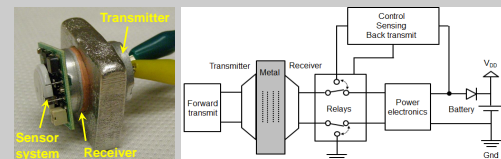
Future work

Improve focusing for phased array transmitter:
- Increase number of transmitter array elements
- Improved array layout to minimize grating lobes
- Pulsed wave excitation to minimize grating lobes

Through metal power & data transfer:
- Demo system entirely embed within metal
- Incorporate phased array focusing

U.S. ARMY RDECOM — **Measuring tip-sample thermal conductance mechanisms for robust quantitative nanoscale thermal analysis via scanning thermal microscopy** — **ARL**

Adam A. Wilson
SEDD, SED-E, Power Components Branch

Motivation and scope

- Quantitatively characterize heat transfer and material thermal properties with nanoscale resolution
- Applications include:
  - Improving efficiency of thermoelectric materials
  - Characterizing behavior of thermally driven MEMS/NEMS
  - Identifying local heat build-up in nanoscale devices
- **Scanning Thermal Microscopy (SThM)** offers best resolution for thermal metrology and requires minimal sample prep and no permanent modification to sample.

Challenges

- Heat transferred between probe and sample is multi-modal (each is dependent on both probe and sample):
  - Across air gap to sample
  - Through water meniscus bridging probe and sample
  - Via solid-solid contact between probe and sample
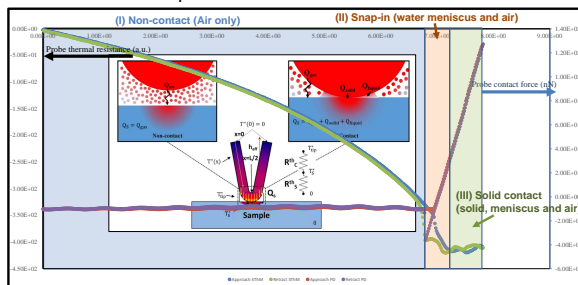
Quantitative measurement is complicated due to co-dependence on each heat transfer mode. **We need a strategy to separately decouple each mode (I, II, and III)!**

Technical Approach

- **(I)** Use **non-contact SThM (NC-SThM)** where only one mode of heat transfer occurs (through air) to determine sample thermal properties.

- 3 unknowns: b, R^{th}_G, k_s
- At diffusive distances: $R^{th}_G = \frac{z}{k_{air}\pi b^2}$
- For reference sample only unknown is b
- With assumed b from calibration, measure samples with unknown k_S

$$b = Az^c$$
$R^2 = 0.99972$
$A = 5.59 \pm 0.16E\text{-}4$ (unitless)
$C = 0.331 \pm 0.002$ (unitless)

- **(II)** Use temperature-dependent **pull-off force volume (FV)** analysis to estimate meniscus thermal conductance

Change in pull-off forces → Wetting angle → Meniscus thermal conductance
$$\Delta F_s \to F_{cap} \to \beta_{wet} \to G^{th}_{H_2O}$$

$$\Delta F_{s,Au} = \to G^{th}_{H_2O,Au} \approx 4\ nW/K$$
$$\Delta F_{s,Glass} = \to G^{th}_{H_2O,Glass} \approx 15\ nW/K$$

- **(III)** Use slope of thermal resistance vs contact force to determine solid-solid contact thermal conductance and probe/sample mechanical properties

Full model for quantitative determination of solid-solid contribution under development

$y = -11.984x - 399.71$
$R^2 = 0.982$

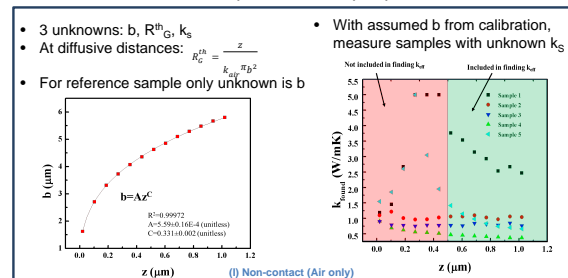$$\frac{\partial R^{th}_P}{\partial F} \to G^{th}_C(P) \to d_C(P) \to (E^*_{Young})\ or\ (H_S))$$

Accomplishments / Future Direction

- Developed technique to decouple probe-sample heat transfer modes using combined non-contact/contact mode SThM, enabling robust quantitative measurements of sample thermal properties and temperature.
- We plan to:
  - Use this strategy to correct signal aberrations in raw data to accurately determine thermal properties of may different materials and devices, including released NEMS structures and nanostructured thermoelectric materials
  - Explore pressure dependence of contact thermal resistances of samples with nanoscale roughness
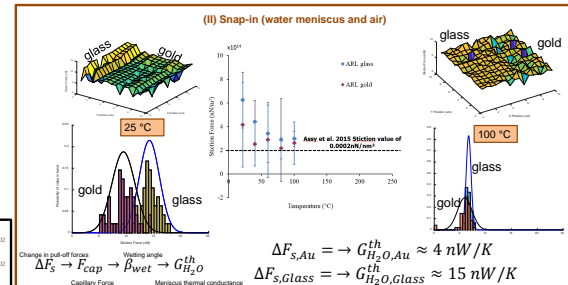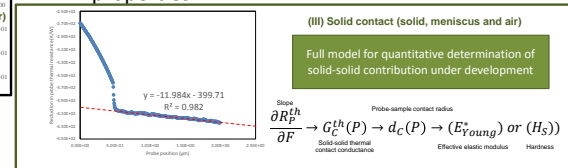
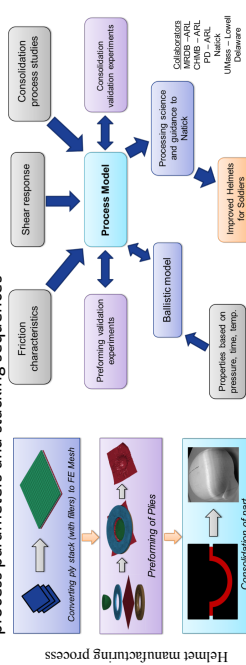# Composite Head Protection Processing Science

Michael Yeager and Travis Bogetti

Weapons and Materials Research Directorate, Weapons and Materials Manufacturing Division, Materials Response and Design Branch

Introduction and Objective

- Companies are currently employing a trail and error approach to thermoplastic composite helmet design
  - Processing science can inform helmet manufacturers of optimal designs and process parameters, eliminating the large time/material cost associated with the trail and error method
  - Goal: To develop a framework for the virtual manufacturing of helmets comprised of extruded UHMWPE films, allowing for the optimization of process parameters and stacking sequences

Converting ply stack (with fillers) to FE Mesh

Preforming of Plies

Consolidation of part

Helmet manufacturing process

Single Curvature Preformer

- A single curvature preformer will be employed to decouple shear and frictional forces from wrinkle formation with manufacturing science objectives that include:
  - Validating the process model
  - Examine how many layers can be homogenized before results are effected
    - 32 sheets sintered in groups of 2, 4, 8, 16, 32
  - Establish a processing strategy and protocol for preforming PE film laminates into parts

Base frame developed with variable dimensions

Preformer design overview

Process Model

Consolidation process studies
Consolidation validation experiments
Shear response
Friction characteristics
Preforming validation experiments
Ballistic model
Properties based on pressure, time, temp.
Processing science and guidance to Natick
Improved Helmets for Soldiers

Collaborators
MRDB – ARL
CHMB – ARL
PD – ARL Natick
UMass – Lowell Delaware

Research Plan

- Process model requires an understanding of complex large scale material deformation
- Simplified models are employed to isolate and investigate critical process parameters

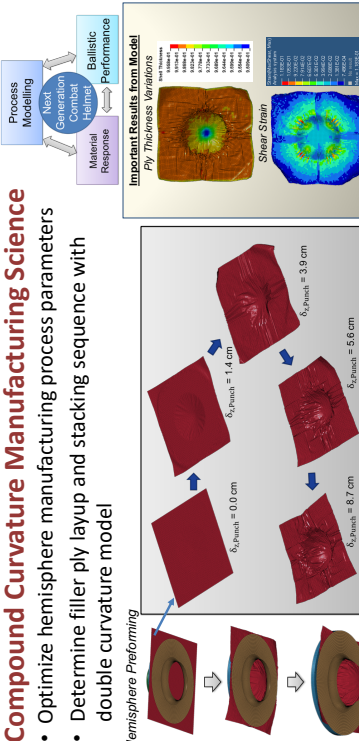|	Characterization Experiments	Simplified Model	Validation Tests	Final Model
Preforming	• Picture frame (T) • Friction tests (TP)	Single curvature	• Bias-extension test (shear, extension coupling) • Multi-ply single curvature forming (bending, friction)	Dual curvature
Consolidation	• Through thickness modulus of plies, elastomer (temperature, rate dependent) F,δ	Consolidation of a flat plate	Compression of flat plate – pressure films at room temperature	Hemi-sphere Compression

Single Curvature Process Model

- Will be utilized to study influence of process parameters and geometric variations such as:
  - Die plate curvature, binder plate, width, etc.
  - Temperature, stroke rate, number of plies
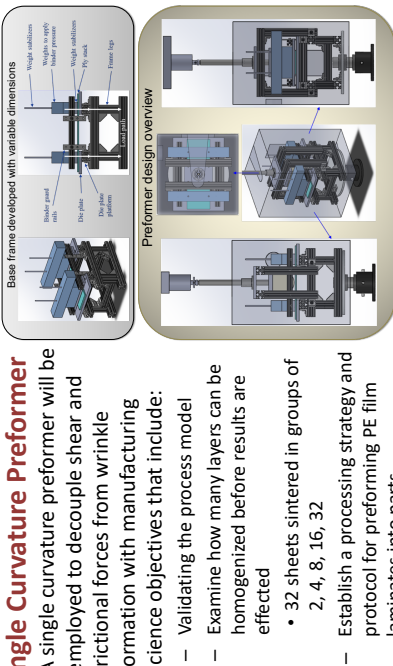 - Including filler plies in the preforming process

Compound Curvature Manufacturing Science

- Optimize hemisphere manufacturing process parameters
- Determine filler ply layup and stacking sequence with double curvature model

Hemisphere Preforming

$\delta_{x,Punch} = 0.0$ cm
$\delta_{x,Punch} = 1.4$ cm
$\delta_{x,Punch} = 3.9$ cm
$\delta_{x,Punch} = 5.6$ cm
$\delta_{x,Punch} = 8.7$ cm

Process Modelling
Next Generation Combat Helmet
Material Response
Ballistic Performance

Important Results from Model

Ply Thickness Variations

Shear Strain

INTENTIONALLY LEFT BLANK.

List of Symbols, Abbreviations, and Acronyms

2PRD   2nd Annual Postdoc Research Day

ARL   US Army Research Laboratory

PDA   postdoc association

CISD   Computational and Information Sciences Directorate

HRED   Human Research and Engineering Directorate

SEDD   Sensors and Electron Devices Directorate

SLAD   Survivability/Lethality Analysis Directorate

WMRD   Weapons and Materials Research Directorate

1	DEFENSE TECHNICAL	43	DIR USARL
(PDF)	INFORMATION CTR	(PDF)	RDRL D
	DTIC OCA		M FLAGG

1
(PDF)

DEFENSE TECHNICAL
INFORMATION CTR
DTIC OCA

2
(PDF)

DIR ARL
IMAL HAR
  RECORDS MGMT
RDRL DCL
  TECH LIB

1
(PDF)

GOVT PRINTG OFC
A MALHOTRA

43
(PDF)

DIR USARL
RDRL D
  M FLAGG
  M HARPER
  P KHOOSHABEHADEH
  A KOTT
  H MAUPIN
  M TSCHOPP
RDRL DS
  T ALEXANDER
RDRL DPT
  J GAMSON
RDRL HR
  P FRANASZCZUK
RDRL WM
  B FORCH
  S KARNA
RDRL VTA
  S NOGAR
RDRL CIE S
  A KALUME
RDRL CII A
  S GUTSTEIN
RDRL CIN T
  A SWAMI
RDRL HRF B
  K DRNEC
RDRL SED E
  M GRAZIANO
  B HANRAHAN
RDRL SED B
  M SMALL
  T ZU
RDRL SED C
  J BOLTERSDORF
  M SCHROEDER
RDRL SED E
  L MAHONEY
  V TSENG
  A WILSON
RDRL SEE E
  K COX
  D GOLTER
RDRL SEE M
  A LLOPIS-JEPSEN
RDRL WML B
  P LAFOND
  R PESCE–RODRIGUEZ
RDRL WML H
  D MAGAGNOSC
RDRL WMM A
  M YEAGER
RDRL WMM B

J CLINE
E HERNANDEZ
RDRL WMM D
C MOCK
RDRL WMM E
N KU
W SHOULDERS
RDRL WMM F
H MURDOCH
RDRL WMM G
D LASTOVICKOVA
M ROENBECK
RDRL WMP B
C HAMPTON
RDRL WMP C
R BECKER
J CLAYTON

INTENTIONALLY LEFT BLANK.